0031-3998/09/6504-0453
PEDIATRIC RESEARCH

Vol. 65, No. 4, 2009
Printed in U.S.A.

Two Novel Mutations in the *ED1* Gene in Japanese Families With X-Linked Hypohidrotic Ectodermal Dysplasia

GUNADI, KENJI MIURA, MIKA OHTA, AKI SUGANO, MYEONG JIN LEE, YUMI SATO, AKIKO MATSUNAGA, KAZUHIRO HAYASHI, TATSUYA HORIKAWA, KAZUNORI MIKI, MARI WATAYA-KANEDA, ICHIRO KATAYAMA, CHIKAKO NISHIGORI, MASAFUMI MATSUO, YUTAKA TAKAOKA, AND HISAHIDE NISHIO

Department of Genetic Epidemiology [G., K.M., M.J.L., H.N.], Laboratory for Applied Genome Science and Bioinformatics [K.M., M.O., A.S., Y.T.], Department of Pediatrics [Y.S., M.M., H.N.], Department of Dermatology [A.M., K.H., T.H., C.H.], Kobe University Graduate School of Medicine, Kobe 650-0017, Japan; Department of Pediatrics [K.M.], Itami Municipal Hospital, Itami 664-8540, Japan; Department of Dermatology [M.W.-K., I.K.], Osaka University Graduate School of Medicine, Suita 565-0871, Japan

ABSTRACT: X-linked hypohidrotic ectodermal dysplasia (XLHED), which is characterized by hypodontia, hypotrichosis, and hypohidrosis, is caused by mutations in *ED1*, the gene encoding ectodysplasin-A (EDA). This protein belongs to the tumor necrosis factor ligand superfamily. We analyzed *ED1* in two Japanese patients with XLHED. In patient 1, we identified a 4-nucleotide insertion, c.119-120insTGTG, in exon 1, which led to a frameshift mutation starting from that point (p.L40fsX100). The patient's mother was heterozygous for this mutation. In patient 2, we identified a novel missense mutation, c.1141G>C, in exon 9, which led to a substitution of glycine with arginine in the TNFL domain of EDA (p.G381R). This patient's mother and siblings showed neither symptoms nor *ED1* mutations, so this mutation was believed to be a *de novo* mutation in maternal germline cells. According to molecular simulation analysis of protein structure and electrostatic surface, p.G381R increases the distance between K375 in monomer A and K327 in monomer B, which suggests an alteration of overall structure of EDA. Thus, we identified two novel mutations, p.L40fsX100 and p.G381R, in *ED1* of two XLHED patients. Simulation analysis suggested that the p.G381R mutation hampers binding of EDA to its receptor *via* alteration of overall EDA structure. **(*Pediatr Res* 65: 453–457, 2009)**

Hypohidrotic ectodermal dysplasia (HED) is a congenital disorder characterized by the impaired development of teeth (hypodontia), hair (hypotrichosis), and eccrine sweat glands (hypohidrosis) (1). Most HED patients have shown an X-linked inheritance pattern, although a minority of patients had an autosomal dominant or recessive trait (2,3).

The *ED1* gene responsible for XLHED was mapped to chromosome Xq12-q13 and was identified by positional cloning (4). *ED1* encodes the protein ectodysplasin-A (EDA) that belongs to the tumor necrosis factor ligand (TNFL) superfamily (5,6). EDA consists of a small N-terminal intracellular domain, a transmembrane domain, and a larger C-terminal extracellular domain containing a furin-cleavage site, a collagen-like domain, and a TNFL domain. The collagen-like domain has been believed to be necessary for trimerization of EDA proteins (7). However, it is not known whether the collagen-like domain is solely responsible for the trimerization: constructs of EDA-A1 and EDA-A2 lacking the collagen-like region can pack in the crystals as dimers of trimers (8). The TNFL domain has the ability to interact with the EDA receptor (EDAR) and X-linked ectodysplasin-A2 receptor (XEDAR) (9).

EDA-A1 and EDA-A2 are the longest EDA isoforms, but they differ by only an insertion/deletion of two amino acids (E308, V309) as determined by alternative splicing of *ED1* pre-mRNA. This insertion/deletion functions to regulate receptor-binding specificity, such that EDA-A1 binds EDAR, whereas EDA-A2 binds XEDAR (10). EDAR interacts with its adapter EDAR-associated death domain (EDARADD) to build an intracellular complex and activate the nuclear factor-κB pathway, which is essential for the proper development of ectodermal derivatives (3,11,12). *EDAR* and *EDARADD* are the genes responsible for the autosomal forms of HED (2,3,13).

Crystal structure analysis has provided a new understanding of EDA-A1 and EDA-A2. For example, higher-order assembly of the EDA trimers has been clarified. The crystallographic asymmetric unit of both EDA-A1 and EDA-A2 crystals contains more than one copy of the biologically relevant trimer. The EDA-A1 asymmetric unit comprises four trimers, and the EDA-A2 asymmetric unit comprises two trimers. Ligation of trimers into higher-order assemblies may increase receptor affinity by avidity or may change the geometry of the ligand-receptor complex (8).

Many mutations in *ED1* in various countries have been reported (14–17). In Japan, several mutations have been identified in XLHED patients (18–20). Affected males showed most or all of the typical phenotypes of XLHED. However, only a few studies have reported the relationship between nucleotide substitution and protein structure (8,21,22).

In this study, we analyzed the *ED1* gene in two unrelated Japanese patients with XLHED, and we identified two novel

Received September 5, 2008; accepted November 4, 2008.
Correspondence: Hisahide Nishio, M.D., Ph.D., Department of Genetic Epidemiology, Kobe University Graduate School of Medicine, 7-5-1 Kusunoki-cho, Chuo-ku, Kobe 650-0017, Japan; e-mail: nishio@med.kobe-u.ac.jp
Supported by a Grant-Aid from the Ministry of Education, Science, Sports and Culture of Japan.

Abbreviations: DHPLC, denaturing high-performance liquid chromatography; **EDA,** ectodysplasin-A; **HED,** hypohidrotic ectodermal dysplasia; **TNFL,** tumor necrosis factor ligand; **XLHED,** X-linked HED

mutations: p.L40fsX100 and p.G381R. The former was inherited from the mother, and the latter was a *de novo* mutation occurred in maternal germline cells. Our molecular simulation analysis of EDA suggested that the p.G381R mutation hampers the binding of EDA to its receptor *via* alteration of the overall structure of EDA.

PATIENTS AND METHODS

Patients. Two Japanese patients with XLHED were enrolled in this study. Informed consent was obtained from the parents before DNA sampling. This study was approved by the Kobe University ethical committee. One hundred healthy Japanese adults volunteered to participate in the study as control subjects.

Patient 1 was a 1-y-5-mo-old boy of unrelated parents in family A (Fig. 2*A*). He had no siblings. The mother was healthy from her appearance; she had no abnormal features and no missing permanent teeth. The patient was initially diagnosed with HED on the basis of his sparse, thin hair; lack of eyebrows and eyelashes; and characteristic facial appearance, including a prominent forehead and saddle nose. The qualitative sweating test with starch and iodine produced almost no response in the patient. The mother showed a slight decrease in sweat response, but she did not undergo further quantitative analysis. Histologic examination of the skin biopsy specimen showed complete lack of hair follicles, eccrine sweat glands, and sebaceous glands, which corresponded to the characteristic findings of HED (Fig. 1A). XLHED was diagnosed on the basis of molecular analysis of *ED1*.

Patient 2 was an 8-mo-old twin boy of unrelated parents in family B (Fig. 3*A*). His elder sister, twin brother, and parents were healthy and showed no dysmorphologic features. He was referred to a city hospital because of recurrent episodes of high temperature. The diagnosis of HED was based on his thin skin, sparse hair; lack of eyebrows; no teeth; and characteristic facial features, including a full forehead and saddle nose. The acetylcholine test demonstrated no sweat response in the patient. Histologic examination of the skin biopsy specimen revealed complete lack of hair follicles, eccrine sweat glands, and sebaceous glands (Fig. 1B). XLHED was diagnosed on the basis of molecular analysis of *ED1*.

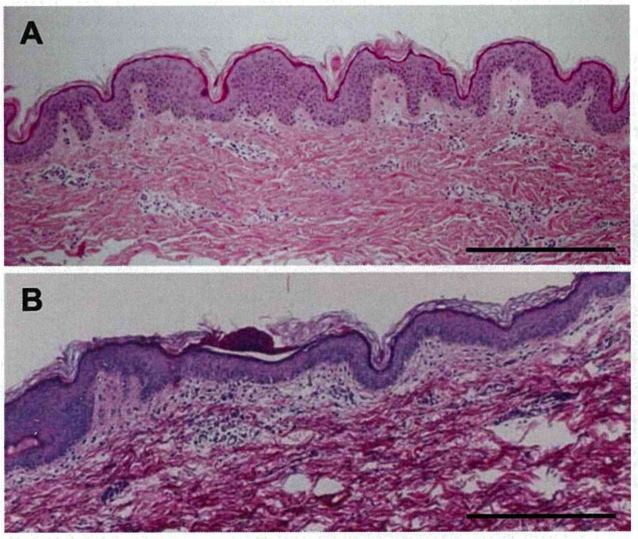

Figure 1. Histologic examination of the skin biopsy specimen. (*A*) Patient 1. H&E staining. Scale bar, 0.5 mm. (*B*) Patient 2. H&E staining. Scale bar, 0.5 mm. Both patients showed complete lack of hair follicles, eccrine sweat glands, and sebaceous glands.

DNA extraction. Genomic DNA was extracted from 2–5 mL of whole blood from each individual by using a DNA extraction kit (SepaGene; Sanko Junyaku, Tokyo, Japan), according to the manufacturer's instructions. The extracted DNA samples were stored at –20°C until analysis.

Polymerase chain reaction. PCR was carried out by using a PC 701 thermal cycler (Astec, Tokyo, Japan). Table 1 shows the primer sequences for *ED1* analysis.

Denaturing HPLC (DHPLC). To screen for a mutation in *ED1*, DHPLC analysis was performed according to our previous reports (23,24). Hybridization of the PCR product mixture of the test DNA with nucleotide substitution and reference DNA without nucleotide substitution produced a heteroduplex peak in the DHPLC chart. The appearance of this heteroduplex peak suggested the presence of a nucleotide substitution in the PCR-amplified fragment. The DHPLC conditions, including column temperatures (Table 1), were determined empirically to maximize resolution of the heteroduplex and homoduplex peaks.

DNA sequencing. To identify and confirm the mutation, direct sequencing analysis was performed with a BigDye Terminator V3.0 Cycle Sequencing Kit (Applied Biosystems, Foster City, CA) and a genetic analyzer (ABI Prism 310; Applied Biosystems), with DNA Sequencing Analysis Software (Applied Biosystems).

Skewed X-chromosome inactivation assay. To determine the X-chromosome inactivation status of the mother of family A, a manifested carrier of XLHED, we quantified the activated and inactivated CpG dinucleotides in exon 1 of the androgen receptor gene (*AR*) by the method described in our previous report (25). To explain briefly, unmethylated (activated) and methylated (inactivated) alleles were measured *via* a combination of DNA digestion by *Hpa*II and PCR amplification of digested and nondigested products. *Hpa*II digested unmethylated CpG but not methylated CpG. PCR amplified only nondigested products, *i.e.* the inactivated allele. The degree of inactivation skewing to one allele was calculated according to the formula presented by Lau *et al.* (26).

Parentage testing. To confirm that all siblings in family B were born to the same parents, parentage testing was performed. Fifteen additional loci on 13 chromosomes were genotyped in all family members by using AmpFLSTR PCR Amplification Kits (Applied Biosystems). The loci tested were D3S1358, vWA, D16S539, D2S1338, D8S1179, D21S11, D18S51, D19S433, THo1, FGA, D5S818, D13S317, D7S820, TPOX, and CSF1PO. Genomic DNA was amplified in a standard PCR reaction, and alleles were analyzed *via* the ABI PRISM 310 Genetic Analyzer with GeneScan and Genotyper software programs (Applied Biosystems).

Molecular simulation analysis of the protein structure and the electrostatic surface. The three-dimensional structures of EDA-A1 and EDA-A2 were derived from Protein Data Bank (accession numbers: EDA-A1, 1RJ7; EDA-A2, 1RJ8). The hydrogen atoms in these model structures were added by means of PyMOL software (27). Following preparation of p.G381R mutants of EDA-A1 and EDA-A2 by means of SWISS-MODEL and Swiss-PDB Viewer (28), the mutant coordinates were optimized by using the MINIMIZE program of the TINKER software package (29) with the AMBER99 force field parameter. The minimizations were executed for root mean square (RMS) gradient values of 0.01 kcal/mol/Å. Then, the molecular structure and electrostatic surface were analyzed by using PyMOL software with the APBS (Adaptive Poisson-Boltzmann Solver) plugin (30).

Table 1. *Primer sets used for amplification of the* ED1 *gene and DHPLC temperature*

Primers name	Forward (5′->3′)	Reverse (5′->3′)	Fragment size (bp)	Annealing temp. (°C)	DHPLC temp (°C)
ED1–1A	TGAACGGCTGAGGCAGACG	TCCGAGCGCAACTCTAGGTA	262	66	62.8
ED1–1B	GCCTGCTCTTCCTGGGTTT	GCCCCTACTAGGTGACTCA	298	58	62.1
ED1–3	TGTTGGCTATGACTGAGTGG	GCCCTACCAAGAAGGTAGTT	248	56	54.0
ED1–4	CTGTGAGACTCCCTCAAATT	ATAACAGACAGACAATGCTGA	257	60	56.4
ED1–5	TGGGCAACAGAGCAGGACT	ACCCACTCCTGCTCTCCTA	306	70	60.4
ED1–6	GAATAAAGCTCAGACAGGGC	AATCTCCGGGGTGTTCTCAT	273	62	58.1
ED1–7	AGGATGGAAACATGGGACTG	AGGGCATGATGGAGCAAAGA	276	62	58.3
ED1–8	CTGTTGCCTCGATTATTCTG	TGCACCGGATCTGCATTCT	242	56	56.9
ED1–9	CACCCTCTCTTTCCTCTCTT	TTAGAGGTTCTGGGAGTCCT	373	60	61.6

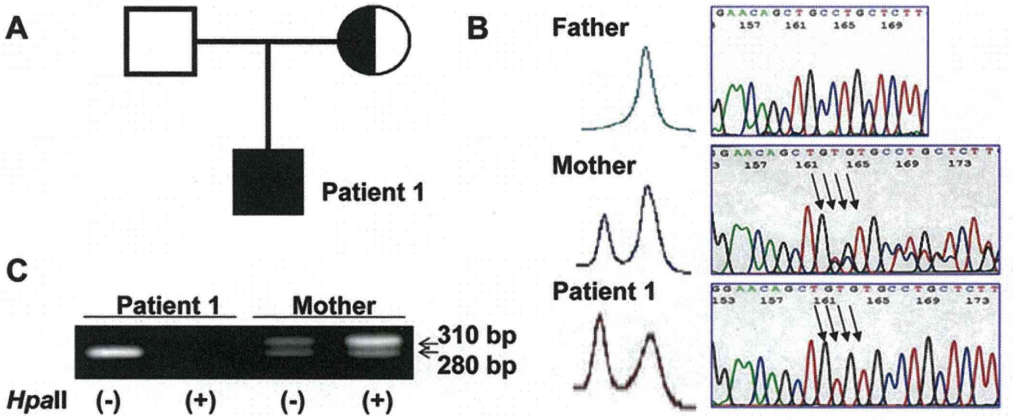

Figure 2. Family A with XLHED. (*A*) Pedigree. (*B*) DHPLC screening and direct DNA sequencing of *ED1* exon 1. The patient carried a c.119-120insTGTG in *ED1* exon 1, which made a premature stop codon at amino acid 100 (p.L40fsX100). His mother was heterozygous for the mutation. Arrows indicate the TGTG insertion. (*C*) X-chromosome inactivation assay. The 310-bp band was from the normal allele, and the 280-bp band was from the affected allele. In patient 1, no amplification of the 280-bp band was obtained, because the patient X-chromosome is not methylated. In his mother, with *Hpa*II treatment produced a higher intensity 310-bp band compared with the 280-bp band, which suggests that the normal allele was mainly inactivated by methylation. The degree of skewed X-chromosome inactivation toward the normal allele was calculated as 80%.

RESULTS

Patient 1 and Family A

Identification of a novel insertion mutation. A heteroduplex peak in the DHPLC chart for *ED1* exon 1 suggested the presence of a mutation in the patient and his mother (Fig. 2*B*). Direct sequencing showed that the patient had a 4-bp insertion between nucleotides 119 and 120 of *ED1* exon 1 (c.119-120insTGTG) (Fig. 2*B*). The mother was heterozygous for the mutation. The insertion c.119-120insTGTG led to a frameshift mutation starting from that point and would result in truncation of the protein at amino acid 100 (p.L40fsX100).

Determination of skewed X-chromosome inactivation. Figure 2*C* shows the result of the skewed X-chromosome inactivation assay. The affected allele of patient 1 was digested completely by *Hpa*II treatment, and no amplification of the 280-bp band of the affected allele was observed. For his mother, two bands, the 310-bp band from the normal allele and the 280-bp band from the affected allele, were obtained with and without *Hpa*II treatment. Without *Hpa*II treatment, the 310-bp and 280-bp bands manifested the same intensity. However, with *Hpa*II treatment, the 310-bp band had a much higher intensity compared with the 280-bp band, which suggests that the normal allele was mainly inactivated by methylation. The degree of skewed X-chromosome inactivation toward the normal allele was calculated to be 80%, *i.e.* only 20% of the activated X-chromosome was normal.

Patient 2 and Family B

Identification of a novel missense mutation. A heteroduplex peak in the DHPLC chart for *ED1* exon 9 suggested the presence of a mutation in the patient (Fig. 3*B*). Direct DNA sequencing showed that the patient had a G-to-C transversion at nucleotide 1141 (Fig. 3*C*). This c.1141G>C transversion led to substitution of glycine with arginine at amino acid 381 (p.G381R) in the TNFL domain. p.G381R likely affects the binding of EDA to its receptor; the glycine residue at amino acid 381 is highly conserved among TNFL domains in TNFL superfamily members (Fig. 3*D*).

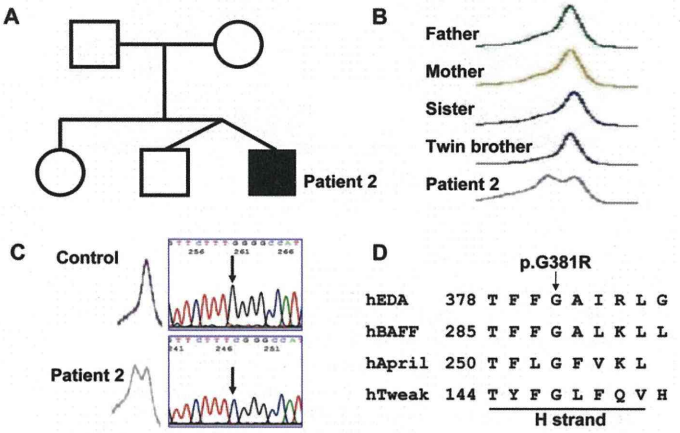

Figure 3. Family B with XLHED. (*A*) Pedigree. (*B*) DHPLC screening of *ED1* exon 9. DHPLC demonstrated a heteroduplex peak for patient 2 but not other family members. (*C*) Direct DNA sequencing of *ED1* exon 9. The patient carried a c.1141G>C in *ED1* exon 9, which led to substitution of glycine with arginine at amino acid 381 (p.G381R). The arrow indicates the c.1141G>C. (*D*) Amino acid sequence alignments of EDA and its closest relatives in the H-strand of the TNFL domain. Bold letters mean conserved amino acids. The glycine at amino acid 381 in EDA is highly conserved among the TNFL superfamily.

DHPLC did not detect the index transversion in family members. The transversion in the patient may be a maternal germline mutation, because parentage testing verified the relationships among family members with a cumulative likelihood ratio of more than 99.99% (data not shown).

To test the possibility that c.1141G>C in *ED1* was a polymorphism, we screened 100 Japanese control subjects for the transversion. None carried this transversion, which suggests that it is not a polymorphism but is instead a disease-causing mutation.

Molecular structure and electrostatic surface of G381R mutants. To investigate whether p.G381R could alter the

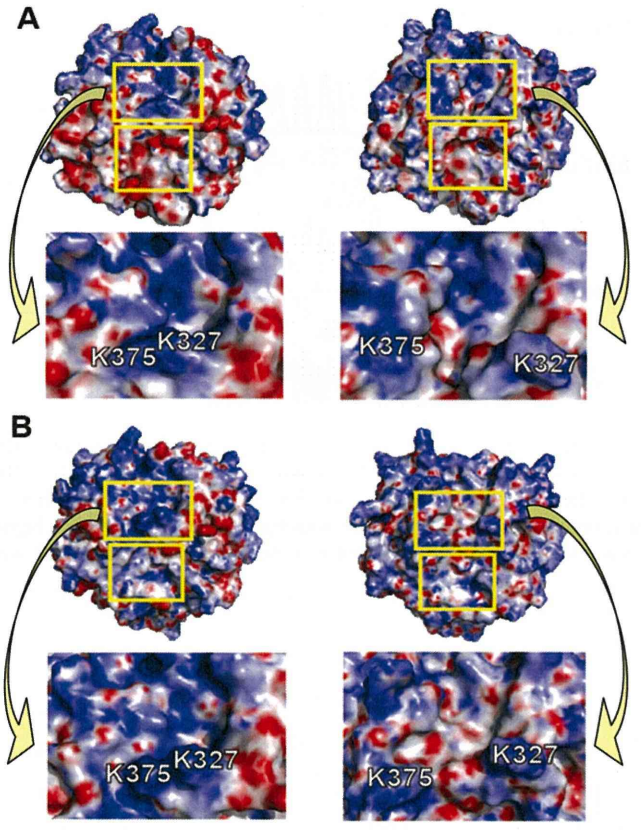

Figure 4. Effect of the p.G381R mutation on the electrostatic surface of EDA-A1 and EDA-A2. (*A*) Electrostatic surfaces of wild-type EDA-A1 (*left*) and p.G381R-mutant EDA-A1 (*right*), with predicted receptor binding sites (*yellow boxes*). As shown in the enlargements of the upper yellow boxed areas, the p.G381R mutation increased the distance between K375 in monomer A and K327 in monomer B. (*B*) Electrostatic surfaces of wild-type EDA-A2 (*left*) and p.G381R-mutant EDA-A2 (*right*), with predicted receptor binding sites (*yellow boxes*). As shown in the enlargements of the upper boxed areas, similar to EDA-A1, the p.G381R mutation increased the distance between K375 in monomer A and K327 in monomer B.

overall structure of EDA, the electrostatic surface and the molecular structure were analyzed by using wild type and simulated mutant molecules. Figure 4*A* and *B* show the molecular surfaces of wild-type and p.G381R-mutated EDA colored according to the calculated electrostatic surface potential. Blue indicates positive (maximum +10 kT/e), white indicates neutral, and red indicates negative (minimum –10 kT/e). The EDA surface contains the putative receptor-binding site along the monomer–monomer interface. The relatively large receptor interaction areas (upper and lower yellow boxes in Fig. 4*A* and *B*) include dispersed binding determinant parts. The mutation alters the positively charged area in the receptor binding sites (upper yellow boxes in Fig. 4*A* and *B*) of EDA. In wild-type isoforms, K375 in monomer A and K327 in monomer B are adjacent, whereas in p.G381R-mutant isoforms, the two amino acids are separated by a considerable distance.

DISCUSSION

Mutations. We identified two novel mutations in *ED1* in two Japanese patients with XLHED. Patient 1 carried a new 4-bp insertion, c.119-120insTGTG, which led to a frameshift mutation starting from amino acid 40 and made a stop codon at amino acid 100 in EDA (p.L40fsX100). The truncated EDA would lack part of the collagen-like domain and the whole TNFL domain. The collagen-like domain is crucial for trimerization of EDA, and the TNFL domain is required for binding of EDA to its receptor (7). However, it is not known whether the collagen-like domain is solely responsible for the trimerization, as described in the Introduction section. Schneider *et al.* (9) also reported that in-frame deletions in collagen-like domain do not affect the ability of EDA to trimerize nor to further multimerize, suggesting that the collagen-like domain may serve additional functions. Thus, the 4-bp insertion may disrupt the functions of the EDA protein because of the loss two important functional domains. Patient 2 carried a novel missense mutation, c.1141G>C, which led to the substitution of glycine with arginine at amino acid 381 in EDA (p.G381R). The mutation is located in the TNFL domain of the EDA protein. Several mutations in the TNFL domain have previously been reported (8,9,22). Schneider *et al.* (9) showed that all missense mutations in the TNFL domain resulted in abolished or impaired binding of EDA to its receptors.

Inheritance traits. The mother of patient 1 had no symptoms except for slightly decreased sweating, with X-chromosome inactivation being skewed mainly toward the normal allele in blood cells. Carriers who are heterozygous for an XLHED mutation may have variable clinical features (14,17,31,32). Lexner *et al.* (17) reported that in two female carriers with pronounced clinical symptoms, the normal allele in their blood cells was mainly inactivated. Martínez *et al.* (31) suggested that skewed X-chromosome inactivation in blood cells can explain symptomatic differences among female carriers. However, the finding for our family A were not consistent with such reports. Our result suggests that X-chromosome inactivation is different in skin from blood cells: ectodermal and mesodermal tissues may differ with regard to factors related to X-chromosome inactivation. It also leads us to the idea that unlike the inference in previous reports, skewed X-chromosome inactivation in blood cells does not predict the clinical situation in the carrier status of XLHED.

The p.G381R mutation in patient 2 was a germline mutation. The recurrence risk of the germline mutation may depend on the proportions of germ cells with and without the mutation (24). The possibility of mutation recurrence in the next male sibling of a patient should be explained to parents during genetic counseling, even though the disease-causing mutation was identified as a *de novo* mutation and the risk of recurrence of the disease cannot be exactly determined.

Protein structure. The p.G381R mutation in patient 2 replaced the small amino acid, glycine, with a larger one, arginine, that could not be accommodated structurally. Hymowitz *et al.* (8) divided the disease-causing mutations that affect the TNFL domain of EDA into three groups: 1) mutations that probably affect the overall structure of EDA, 2) mutations that affect the receptor binding site, and 3) mutations whose effect is uncertain but that may define a novel interaction site. It is most reasonable to expect that p.G381R belongs to the first group and may affect EDA function *via* alteration of overall EDA structure. Our simulation data offered some evidence for this hypothesis. The mutation in-

creased the distance between K375 in monomer A and K327 in monomer B, which resulted in a drastic change in the electrostatic surface and surface conformation of the receptor binding site (upper boxes in Fig. 4*A* and *B*).

The question then arises: how does this p.G381R-induced alteration in structure affect EDA function? One possible explanation is that the electrostatic and structural changes in the surface caused by the mutation may hamper receptor binding. It should be noted that the mutation produced a large alteration in the "upper box" part of the receptor-binding site and a small alteration in the "lower box" part. This finding suggests that these parts of the receptor-binding site play different roles, that is, maintaining binding affinity and providing the receptor specificity, respectively. Another possible explanation is that unexpected physiochemical changes related to p.G381R may have a negative effect on receptor binding or assembly of the three monomers. An additional possibility is that the mutation alters the solubility or folding properties of EDA, which are related to its secretion by cells.

In conclusion, we found two novel mutations, one a frameshift (p.L40fsX100) and one a missense (p.G381R), in *ED1* and discussed their inheritance trait in two unrelated families with XLHED. Molecular simulation analysis of the structure of the EDA protein suggested that the missense mutation hampers the binding of EDA into its receptor *via* alteration of the overall structure of EDA.

Acknowledgments. We thank Dr. Ahmad Hamim Sadewa and Dr. Teguh Haryo Sasongko (Kobe University Graduate School of Medicine) for their technical assistance and Drs. Surini Yusoff and Indra Sari Kusuma Harahap (Kobe University Graduate School of Medicine) for their helpful comments on interpretation of the data.

REFERENCES

1. McKusick VA 1998 Mendelian Inheritance in Man, 12th Ed. Johns Hopkins University Press, Baltimore, pp 3307–3309
2. Monreal AW, Ferguson BM, Headon DJ, Street SL, Overbeek PA, Zonana J 1999 Mutations in the human homologue of mouse *dl* cause autosomal recessive and dominant hypohidrotic ectodermal dysplasia. Nat Genet 22:366–369
3. Headon DJ, Emmal SA, Ferguson BM, Tucker AS, Justice MJ, Sharpe PT, Zonana J, Overbeek PA 2001 Gene defect in ectodermal dysplasia implicates a death domain adapter in development. Nature 414:913–916
4. Kere J, Srivastava AK, Montonen O, Zonana J, Thomas N, Ferguson B, Munoz F, Morgan D, Clarke A, Baybayan P, Chen EY, Ezer S, Saarialho-Kere U, de la Chapelle A, Schlessinger D 1996 X-linked anhidrotic (hypohidrotic) ectodermal dysplasia is caused by mutation in a novel transmembrane protein. Nat Genet 13:409–416
5. Bayés M, Hartung AJ, Ezer S, Pispa J, Thesleff I, Srivastava AK, Kere J 1998 The anhidrotic ectodermal dysplasia gene (EDA) undergoes alternative splicing and encodes ectodysplasin-A with deletion mutations in collagenous repeats. Hum Mol Genet 7:1661–1669
6. Monreal AW, Zonana J, Ferguson B 1998 Identification of a new splice form of the EDA1 gene permits detection of nearly all X-linked hypohidrotic ectodermal dysplasia mutations. Am J Hum Genet 63:380–389
7. Ezer S, Bayés M, Elomaa O, Schlessinger D, Kere J 1999 Ectodysplasin is a collagenous trimeric type II membrane protein with a tumor necrosis factor-like domain and co-localizes with cytoskeletal structures at lateral and apical surfaces of cells. Hum Mol Genet 8:2079–2086
8. Hymowitz SG, Compaan DM, Yan M, Wallweber HJ, Dixit VM, Starovasnik MA, de Vos AM 2003 The crystal structures of EDA-A1 and EDA-A2: splice variants with distinct receptor specificity. Structure 11:1513–1520
9. Schneider P, Street SL, Gaide O, Hertig S, Tardivel A, Tschopp J, Runkel L, Alevizopoulos K, Ferguson BM, Zonana J 2001 Mutations leading to X-linked hypohidrotic ectodermal dysplasia affect three major functional domains in the tumor necrosis factor family member ectodysplasin-A. J Biol Chem 276:18819–18827
10. Yan M, Wang LC, Hymowitz SG, Schilbach S, Lee J, Goddard A, de Vos AM, Gao WQ, Dixit VM 2000 Two-amino acid molecular switch in an epithelial morphogen that regulates binding to two distinct receptors. Science 290:523–527
11. Yan M, Zhang Z, Brady JR, Schilbach S, Fairbrother WJ, Dixit VM 2002 Identification of a novel death domain-containing adaptor molecule for ectodysplasin-A receptor that is mutated in crinkled mice. Curr Biol 12:409–413
12. Mikkola ML, Thesleff I 2003 Ectodysplasin signaling in development. Cytokine Growth Factor Rev 14:211–224
13. Bal E, Baala L, Cluzeau C, El Kerch F, Ouldim K, Hadj-Rabia S, Bodemer C, Munnich A, Courtois G, Sefiani A, Smahi A 2007 Autosomal dominant anhidrotic ectodermal dysplasias at the EDARADD locus. Hum Mutat 28:703–709
14. Vincent MC, Biancalana V, Ginisty D, Mandel JL, Calvas P 2001 Mutational spectrum of the ED1 gene in X-linked hypohidrotic ectodermal dysplasia. Eur J Hum Genet 9:355–363
15. Visinoni AF, de Souza RL, Freire-Maia N, Gollop TR, Chautard-Freire-Maia EA 2003 X-linked hypohidrotic ectodermal dysplasia mutations in Brazilian families. Am J Med Genet A 122:51–55
16. Zhao J, Hua R, Zhao X, Meng Y, Ao Y, Liu Q, Shang D, Sun M, Lo WH, Zhang X 2008 Three novel mutations of the EDA gene in Chinese patients with X-linked hypohidrotic ectodermal dysplasia. Br J Dermatol 158:614–617
17. Lexner MO, Bardow A, Juncker I, Jensen LG, Almer L, Kreiborg S, Hertz JM 2008 X-linked hypohidrotic ectodermal dysplasia. Genetic and dental findings in 67 Danish patients from 19 families. Clin Genet 74:252–259
18. Yotsumoto S, Fukumaru S, Matsushita S, Oku T, Kobayashi K, Saheki T, Kanzaki T 1998 A novel point mutation of the EDA gene in a Japanese family with anhidrotic ectodermal dysplasia. J Invest Dermatol 111:1246–1247
19. Aoki N, Ito K, Tachibana T, Ito M 2000 A novel arginine → serine mutation in EDA1 in a Japanese family with X-linked anhidrotic ectodermal dysplasia. J Invest Dermatol 115:329–330
20. Hashiguchi T, Yotsumoto S, Kanzaki T 2003 Mutations in the ED1 gene in Japanese families with X-linked hypohidrotic ectodermal dysplasia. Exp Dermatol 12:518–522
21. RamaDevi AR, Reddy EC, Ranjan S, Bashyam MD 2008 Molecular genetic analysis of patients from India with hypohidrotic ectodermal dysplasia reveals novel mutations in the EDA and EDAR genes. Br J Dermatol 158:163–167
22. Li S, Li J, Cheng J, Zhou B, Tong X, Dong X, Wang Z, Hu Q, Chen M, Hua ZC 2008 Non-syndromic tooth agenesis in two Chinese families associated with novel missense mutations in the TNF domain of EDA (ectodysplasin A). PLoS One 3:e2396
23. Sutomo R, Akutsu T, Takeshima Y, Nishio H, Sadewa AH, Harada Y, Matsuo M 2002 Rapid SMN1 deletion test using DHPLC to screen patients with spinal muscular atrophy. Am J Med Genet 113:225–226
24. Sadewa AH, Sasongko TH, Gunadi, Lee MJ, Daikoku K, Yamamoto A, Yamasaki T, Tanaka S, Matsuo M, Nishio H 2008 Germ-line mutation of KCNQ2, p.R213W, in a Japanese family with benign familial neonatal convulsion. Pediatr Int 50:167–171
25. Ishihara H, Kanda F, Nishio H, Sumino K, Chihara K 2001 Clinical features and skewed X-chromosome inactivation in female carriers of X-linked recessive spinal and bulbar muscular atrophy. J Neurol 248:856–860
26. Lau AW, Brown CJ, Peñaherrera M, Langlois S, Kalousek DK, Robinson WP 1997 Skewed X-chromosome inactivation is common in fetuses or newborns associated with confined placental mosaicism. Am J Hum Genet 61:1353–1361
27. DeLano WL 2002 The PyMOL Molecular Graphics System. Available at: http://www.pymol.org Accessed August 30, 2008
28. Guex N, Peitsch MC 1997 SWISS-MODEL and the Swiss-PdbViewer: an environment for comparative protein modeling. Electrophoresis 18:2714–2723
29. Ren P, Ponder JW 2003 Polarizable atomic multipole water model for molecular mechanics simulation. J Phys Chem B 107:5933–5947
30. Baker NA, Sept D, Joseph S, Holst MJ, McCammon JA 2001 Electrostatics of nanosystems: application to microtubules and the ribosome. Proc Natl Acad Sci USA 98:10037–10041
31. Martínez F, Millán JM, Orellana C, Prieto F 1999 X-linked anhidrotic (hypohidrotic) ectodermal dysplasia caused by a novel mutation in EDA1 gene: 406T>G (Leu55Arg). J Invest Dermatol 113:285–286
32. Vincent MC, Cossée M, Vabres P, Stewart F, Bonneau D, Calvas P 2002 Pitfalls in clinical diagnosis of female carriers of X-linked hypohidrotic ectodermal dysplasia. Arch Dermatol 138:1256–1258

J Cutan Pathol 2009: 36: 517–521
doi: 10.1111/j.1600-0560.2008.01086.x
John Wiley & Sons. Printed in Singapore

Journal of
Cutaneous Pathology

Reduction in QSART and vasoactive intestinal polypeptide expression in the skin of Parkinson's disease patients and its relation to dyshidrosis

Background: With regards to dyshidrosis in Parkinson's disease (PD), there is no established and consistent view on the occurrence sites, frequency and etiology, although there have been several reports on hypohidrosis of the limbs and sudoresis on the face/cervical region.
Methods: Hydrosis in the forearms of PD patients and healthy individuals were compared by quantitative sudomotor axon reflex test (QSART). The expression of various neuropeptides and α-synuclein was examined with immunohistochemical staining.
Results: There was a significant reduction in QSART of PD patients but not of healthy controls. Reduced expression of vasoactive intestinal polypeptide (VIP) was also detected in the sweat glands of PD patients.
Conclusion: Reduction in QSART and VIP expression in the sweat glands might be involved in the dyshidrosis of PD patients.

Kawada M, Tamada Y, Simizu H, Yanagishita T, Yamashita N, Ishida N, Watanabe D, Yoshida M, Ibi T, Sahashi K, Hashizume Y, Matsumoto Y. Reduction in quantitative sudomotor axon reflex test and vasoactive intestinal polypeptide expression in the skin of Parkinson's disease patients and its relation to dyshidrosis.
J Cutan Pathol 2009; 36: 517–521. © 2009 John Wiley & Sons A/S.

Morihiro Kawada[1], Yasuhiko Tamada[1], Hirokazu Simizu[1], Takeshi Yanagishita[1], Noriko Yamashita[1], Natsuko Ishida[1], Daisuke Watanabe[1], Mari Yoshida[3], Tatsu Ibi[2], Kou Sahashi[2], Yoshio Hashizume[3] and Yoshinari Matsumoto[1]

[1]Department of Dermatology,
[2]Department of Neurology, Aichi Medical University School of Medicine, Nagakute, Aichi, Japan
[3]Department of Neurology, Institute for Medical Science of Aging, Aichi Medical University School of Medicine, Nagakute, Aichi, Japan

Daisuke Watanabe, Department of Dermatology, Aichi Medical University School of Medicine, Nagakute, Aichi 480-1195, Japan
Tel: +81 (52) 264-4811
Fax: +81 (561) 63-9914
e-mail: dwatanab@aichi-med-u.ac.jp

Accepted for publication May 18, 2008

Although dyshidrosis is widely known as one of the autonomic disorders in Parkinson's disease (PD), the frequency of the disorder varies among investigators' reports. Appenzeller et al.[1] and Aminoff et al.[2] found 10 disorders (53%) of 19 patients and 6 (54%) of 11 patients, respectively. Sandroni et al.[3] reported dyshidrosis in less than 40% of 35 PD patients. Thaisetthawatkul et al.[4] reported that PD patients had the mildest degree of the disorder. However, Kihara et al.[5] failed to show significant changes in hydrosis of PD patients. The varied frequency of incidence and intensity of dyshidrosis might be because of difference in techniques used or in disease stages of PD patients.

Sweat production is regulated by autonomic neural system, and the dyshidrosis in PD is suggested to be caused by autonomic neural disturbance, especially sympathetic nervous system.[6] Sweat gland is innervated by cholinergic sympathetic neurons.[7] The sympathetic nerve-dependent sweat production can be analyzed by a quantitative sudomotor axon reflex tests (QSART).[8] Immunohistochemical studies have identified a number of possible peptide neuromodulators (e.g. vasoactive intestinal polypeptide, VIP) in and around cholinergic sudomotor nerve terminals and eccrine sweat glands.[9,10] In this study, we examined dyshidrosis of PD patients with QSART on sympathetic nerve functions. We also examined the

expression of neuropeptides and α-synuclein, which affect sympathetic nerve functions, in the sweat glands of the patients with immunohistochemical staining.

Materials and methods

Subjects

Twelve PD patients who were under the care of the Department of Neurological Medicine in Aichi Medical University Hospital were the subjects. Of these, six patients were males (mean age 69.8 years) and six were females (mean age 69.7 years). The mean disease duration was 103.3 months. The control group consisted of six patients without a skin rash on the forearm, three males (mean age 66 years) and three females (mean age 67 years), who are under the care of the Department of Dermatology in the hospital. In addition, autopsy samples from three patients (two males and one female with a mean age of 72.8 years), who were pathologically diagnosed for having PD or diffuse Lewy body disease from 1995 to 2003 in the Institute for Aging, were utilized for staining of the sympathetic ganglia. All experiments were carried out under the consent of the patients and healthy controls.

Quantitative sudomotor axon reflex test

QSART was used to examine the integrity of post-ganglionic sympathetic cholinergic innervation of sweat glands.[7] Sweat production is measured in an adjacent area by the increase in relative humidity in an airtight chamber. Briefly, 10% acetylcholine was made to infiltrate the measurement site on the right forearm by iontophoresis for 5 min at 1 mA electric current, and the amount for the axon reflex sweating was quantified by using the capsule ventilation technique. This was recorded for 10 min as the axon reflex-mediated sweat response. Amount of perspiration (mg/10 min) is expressed as the mean ± SD. The statistical significance of differences was determined by unpaired Student's *t*-test. A $p < 0.05$ vs. control subjects was considered statistically significant.

Immunohistochemistry

Among 12 patients who were subjected to QSART, 3-mm punch biopsy specimens were obtained from the forearm flexor surface of 11 patients consented to this procedure. The specimens were fixed with formalin and stained with hematoxylin and eosin. They were also stained immunohistochemically with antibodies against the following antigens: neuron-specific enolase (NSE), protein gene product 9.5 (PGP9.5), choline acetyltransferase (ChAT), calcitonine gene-related peptide (CGRP) and VIP. After deparaffinization, the specimens were treated with 30% hydrogen peroxide, reacted with each primary antibody (Table 1) at 4°C for 24 h and stained using the labeled streptavidin-biotin method (DAKO, Glostrup, Denmark) according to manufacturer's protocol. Nuclei were stained with Mayer's hematoxylin. Three to five sweat gland secretory portions per specimen were observed under a microscope and the

Table 1. The list of antibodies used for immunohistochemical studies

Antibody	Source	Dilution used
NSE	Dako	1 : 200
PGP9.5	Dako	1 : 100
ChAT	Chemicon (CA, USA)	1 : 100
CGRP	Sigma (Mi, USA)	1 : 100
VIP	Sigma (Mi, USA)	1 : 100
α-Syn	Santa Cruz (CA, USA)	1 : 200
p-α-Syn	Wako (Osaka, Japan)	1 : 2000

α-Syn, α-synuclein; CGRP, P-α-Syn, phosphorylated α-synuclein; calcitonine gene-related peptide; ChAT, choline acetyltransferase; NSE, neuron-specific enolase; PGP, protein gene product; VIP, vasoactive intestinal polypeptide.

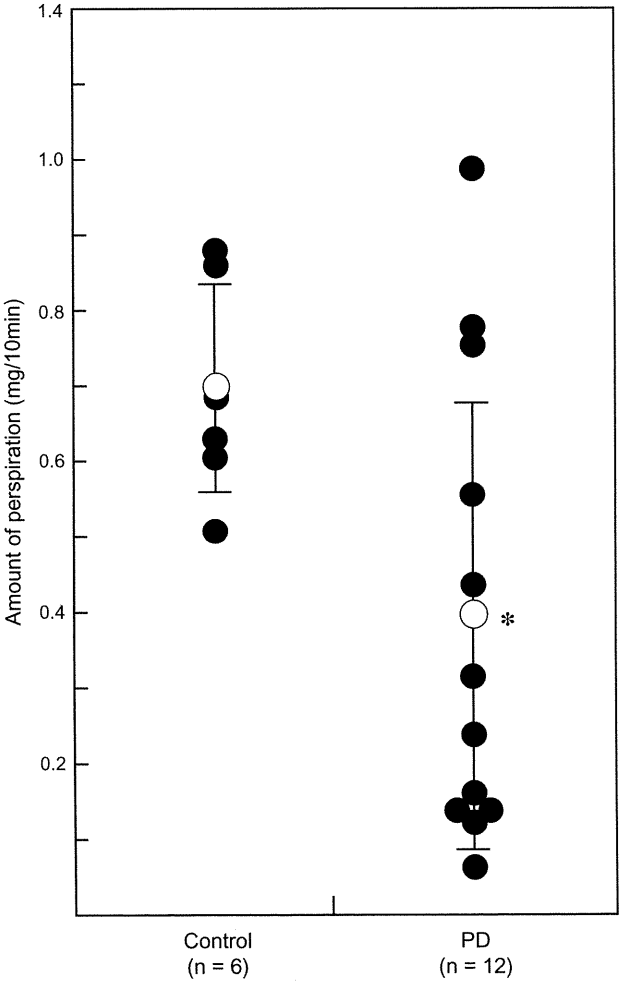

Fig. 1. Quantitative sudomotor axon reflex test. Axon reflex sweating of the upper limbs in Parkinson's disease patients and controls were examined ●. Amount of perspiration is expressed as the mean (white circle) ± SD. *$p < 0.05$ vs. control subjects.

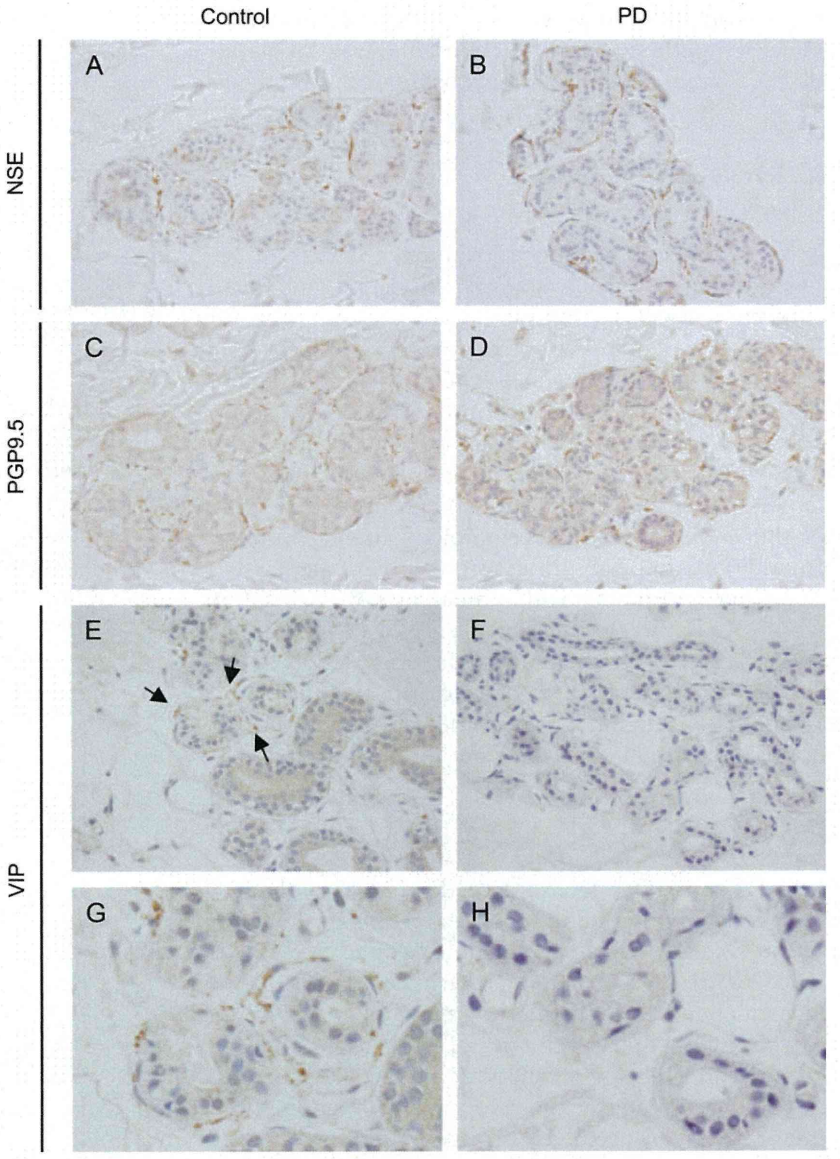

Fig. 2. Expression of neuropeptides in the sweat glands was examined with immunohistochemical staining. Original magnification: (A–F) ×400; (G and H) ×1000. NSE, neuron-specific enolase; PD, Parkinson's disease; PGP, protein gene product; VIP, vasoactive intestinal polypeptide.

staining was scored as negative (−), weak positive (±) or positive (+) based on the number of positive cells.[8] Formalin-fixed and paraffin-embedded sections (9 μm) of the autopsied sympathetic ganglia of the three PD patients and three control patients were immunohistochemically stained with anti-α-synuclein antibody and anti-phosphorylated α-synuclein antibody. Similar staining was also performed with the 4-μm skin sections.

Results

Quantitative sudomotor axon reflex test

QSART was carried out in 12 PD patients and six healthy controls (Fig. 1). Reduction in QSART was observed in 7 of 12 PD patients. The axon reflex sweating on the upper limbs of PD patients was significantly low compared with the case of the control subjects ($p < 0.05$).

Histology of the sweat glands

The histology of the sweat glands of PD patients and healthy controls was observed under a microscope. Neither the atrophy of the sweat gland secretory portions nor the constriction of the ducts was observed in PD patients (data not shown). There was no histological difference in the sweat glands between PD patients and the healthy controls.

Expression of neuropeptides in the sweat glands

The expression of various neuropeptides was examined immunohistochemically in the sweat glands of PD

Table 2. Comparison of the reduction in QSQRT and VIP expression

Patient	Sex	QSART perspiration (mg/10 min)	VIP staining
1	F	0.06	−
2	M	0.13	±
3	F	0.15	−
4	M	0.15	−
5	F	0.25	±
6	M	0.32	−
7	M	0.43	−
8	F	0.54	±
9	F	0.76	−
10	F	0.78	−
11	M	1.00	−

−, negative; ±, 1–4 positive cells; +, more than five positive cells; F, female; M, male; QSART, quantitative sudomotor axon reflex test; VIP, vasoactive intestinal polypeptide.

patients (Fig. 2). In the NSE and PGP9.5 staining, both PD and control specimens showed a nerve fiber distribution pattern, which surrounds the sweat gland secretory portion in a ring shape (Fig. 2A–D). The sweat gland secretory portions in PD patients and control samples were positively stained with ChAT and CGRP staining and there was no significant difference in those staining patterns. However, no VIP expression was detected in 8 of 11 PD specimens (Fig. 2E–H), and reduced VIP expression was detected at nerve fibers around the sweat gland secretory portion in 3 of 11 PD specimens. In addition, there was no statistical correlation between the reduction score of QSART and the reduction intensity of VIP staining in PD patients. The relationship between intensities of VIP staining and QSART levels is shown in Table 2.

Accumulation of α-synuclein

The expression of α-synuclein was examined immunohistochemically in thoracic sympathetic ganglion and sweat glands of PD patients. Nerve cells and nerve cell bodies of the sympathetic ganglia in the PD autopsy specimens were positively stained with anti-phosphorylated α-synuclein antibody (Fig. 3A) and anti-α-synuclein antibody (data not shown). However, no positive staining was observed in skin specimens collected from the forearms of the 11 PD patients and autopsied control patients (Fig. 3B–D). The summary of the immunohistochemical stainings is shown in Table 3.

Discussion

In this study, we show the reduction in QSART and VIP expression in the sweat glands of PD patients. The reduction in QSART and VIP expression might be involved in the dyshidrosis of PD patients. QSART is a sympathetic nerve-dependent hidrosis testing method devised by Low et al., which was judged to be excellent in objectivity and reproducibility by the American Academy of Neurology.[11] The reduction in QSART suggests the involvement of altered sympathetic nerve function in the dyshidrosis of PD patients. This study shows the reduced sweating function on the forearm in 6 of 12 PD patients. There are already several reports on the dyshidrosis of PD patients,[1–5] although the frequency and intensity varied in those reports.

Reduced VIP expression is seen in the nerves distributed around the secretory portion of the PD specimens. VIP is normally expressed in the dermal vessels and the nerves around the sweat gland secretory portion and plays an important role in hidrosis along with acetylcholine.[12] Using eccrine sweat glands separated from a Rhesus monkey's palm, Sato et al.[13] reported that VIP induces eccrine perspiration and that it accumulates cyclic adenosine mono-phosphate

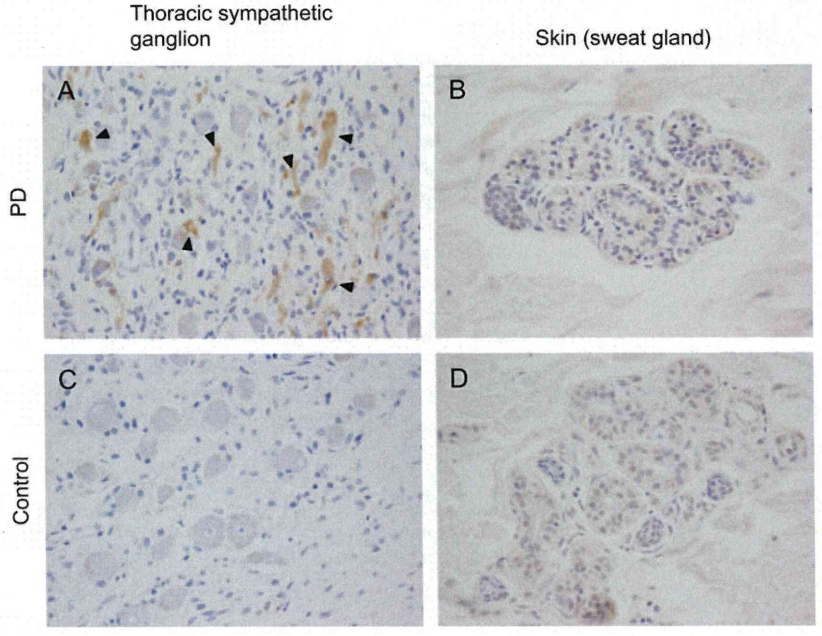

Fig. 3. A–D) Expression of α-synuclein in the sweat glands was examined with immunohistochemical staining. Original magnification ×400. PD, Parkinson's disease.

Table 3. The summary of immunohistochemical staining

		Neuropeptide						
	Tissue	NSE	PGP	ChAT	CGRP	VIP	α-Syn	p-α-Syn
Control	Skin	+	+	+	±	+	−	−
	Thoracic sympathetic ganglion						−	−
Parkinson's disease	Skin	+	+	+	±	−~± (3/11: ±) (8/11: −)	−	−
	Thoracic sympathetic ganglion						+	+

α-Syn, α-synuclein; P-α-Syn, phosphorylated α-synuclein; CGRP, calcitonine gene-related peptide; ChAT, choline acetyltransferase; PGP, protein gene product; NSE, neuron-specific enolase; VIP, vasoactive intestinal polypeptide.

(AMP) in the secretory cells and increases the secretion of sweat. Moreover, Tainio[14] confirmed that VIP activates adenylate cyclase even without synergy from acetylcholine in the human sweat glands and promotes cyclic adenosine mono-phosphate (cAMP) production from adenosine tri-phosphate (ATP). Further, the relationship between dyshidrosis and reduced VIP expression is known in several diseases.[15,16] Based on those findings, the reduced VIP expression in the sweat glands of PD patients might be related to the altered sympathetic nerve function, assessed by QSART.

The appearance of Lewy bodies in the sympathetic nervous system leads to autonomic nervous system dysfunction.[17–19] No deposit of α-synuclein was observed in the sweat glands of PD patients, although it was observed in the nerve cells and neurites of the thoracic sympathetic ganglia. In this study, we could not obtain the evidence on the dysfunction of sympathetic nerves in the sweat glands by α-synuclein. However, a possibility is not excluded that the accumulation of α-synuclein in the thoracic sympathetic ganglia might play a role on the dyshidrosis in PD.

Neither the atrophy of the sweat gland secretory portions nor the constriction of the ducts was seen in the sweat glands of PD patients. There was no significant difference in the histology of the sweat glands between PD patients and healthy controls. Therefore, the dyshidrosis of PD might be responsible for functional disorder of the perspiration nerve. It is also supported by the reduction in QSART and VIP expression.

Acknowledgements

We thank A. Morikawa, K. Kohtani and T. Mizuno for excellent technical assistance during the course of this study.

References

1. Appenzeller O, Gross JE. Autonomic deficits in Parkinson's syndrome. Arch Neurol 1971; 24: 50.
2. Aminoff MJ, Willcox CS. Assessment of autonomic function in patients with a Parkinsonian syndrome. Br Med J 1971; 4: 80.
3. Sandroni P, Ahlskog JE, Fealey RD, Low PA. Autonomic involvement in extrapyramidal and cerebellar disorders. Clin Auton Res 1991; 1: 147.
4. Thaisetthawatkul P, Boeve BF, Benarroch EE, et al. Autonomic dysfunction in dementia with Lewy bodies. Neurology 2004; 62: 1804.
5. Kihara M, Kihara Y, Tukamoto T, et al. Assessment of sudomotor dysfunction in early Parkinson's disease. Eur Neurol 1993; 33: 363.
6. Hirayama M. Sweating dysfunctions in Parkinson's disease. J Neurol 2006; 253: 42.
7. Ernsberger U, Rohrer H. Development of the cholinergic neurotransmitter phenotype in postganglionic sympathetic neurons. Cell Tissue Res 1999; 297: 339.
8. Braune C, Erbguth F, Birklein F. Dose thresholds and duration of the local anhidrotic effect of botulinum toxin injections: measured by sudometry. Br J Dermatol 2001; 144: 111.
9. Tainio H, Vaalasti A, Rechadt L. The distribution of substance P-, CGRP-, galanin- and ANP-like immunoreactive nerves in human sweat glands. Histochem J 1987; 19: 375.
10. Shibasaki M, Wilson TE, Crandall CG. Neural control and mechanisms of eccrine sweating during heat stress and exercise. J Appl Physiol 2006; 100: 1692.
11. Low PA, Caskey PE, Tuck RR, Fealey RD, Dyck PJ. Quantitative sudomotor axon reflex test in normal and neuropathic subjects. Ann Neurol 1983; 14: 573.
12. Lotti T, Hautmann G, Panconesi E. Neuropeptides in skin. J Am Acad Dermatol 1995; 33: 482.
13. Sato K, Sato F. Effect of VIP on sweat secretion and cAMP accumulation in isolated simian eccrine glands. Am J Physiol 1987; 253: R935.
14. Tainio H. Cytochemical localization of VIP-stimulated adenylate cyclase activity in human sweat glands. Br J Dermatol 1987; 116: 323.
15. Properzi G, Francavilla S, Poccia G, et al. Early increase precedes a depletion of VIP and PGP-9.5 in the skin of insulin-dependent diabetics – correlation between quantitative immunohistochemistry and clinical assessment of peripheral neuropathy. J Pathol 1993; 169: 269.
16. Nolano M, Provitera V, Perretti A, et al. Ross syndrome: a rare or a misknown disorder of thermoregulation? A skin innervation study on 12 subjects. Brain 2006; 129: 2119.
17. Den Hartog Jager WA, Bethlem J. The distribution of Lewy bodies in the central and peripheral autonomic nervous systems in idiopathic paralysis agitans. J Neurol Neurosurg Psychiatry 1960; 23: 283.
18. Rajput AH, Rozdilsky B. Dysautonomia in Parkinsonism: a clinicopathological study. J Neurol Neurosurg Psychiatry 1976; 39: 1092.
19. Hague K, Lento P, Morgello S, Caro S, Kaufmann H. The distribution of Lewy bodies in pure autonomic failure: autopsy findings and review of the literature. Acta Neuropathol 1997; 94: 192.

THE JOURNAL OF BIOLOGICAL CHEMISTRY VOL. 285, NO. 52, pp. 40777–40784, December 24, 2010

Phosphorylation of Aquaporin-2 Regulates Its Water Permeability*

Received for publication, June 4, 2010, and in revised form, October 16, 2010 Published, JBC Papers in Press, October 22, 2010, DOI 10.1074/jbc.M110.151928

Kayoko Eto‡, Yumi Noda‡[1], Saburo Horikawa§, Shinichi Uchida‡, and Sei Sasaki‡

From the ‡Department of Nephrology and §Division of Pathophysiology, Tokyo Medical and Dental University, Tokyo 113-8519, Japan

Vasopressin-regulated water reabsorption through the water channel aquaporin-2 (AQP2) in renal collecting ducts maintains body water homeostasis. Vasopressin activates PKA, which phosphorylates AQP2, and this phosphorylation event is required to increase the water permeability and water reabsorption of the collecting duct cells. It has been established that the phosphorylation of AQP2 induces its apical membrane insertion, rendering the cell water-permeable. However, whether this phosphorylation regulates the water permeability of this channel still remains unclear. To clarify the role of AQP2 phosphorylation in water permeability, we expressed recombinant human AQP2 in *Escherichia coli*, purified it, and reconstituted it into proteoliposomes. AQP2 proteins not reconstituted into liposomes were removed by fractionating on density step gradients. AQP2-reconstituted liposomes were then extruded through polycarbonate filters to obtain unilamellar vesicles. PKA phosphorylation significantly increased the osmotic water permeability of AQP2-reconstituted liposomes. We then examined the roles of AQP2 phosphorylation at Ser-256 and Ser-261 in the regulation of water permeability using phosphorylation mutants reconstituted into proteoliposomes. The water permeability of the non-phosphorylation-mimicking mutant S256A-AQP2 and non-phosphorylated WT-AQP2 was similar, and that of the phosphorylation-mimicking mutant S256D-AQP2 and phosphorylated WT-AQP2 was similar. The water permeability of S261A-AQP2 and S261D-AQP2 was similar to that of non-phosphorylated WT-AQP2. This study shows that PKA phosphorylation of AQP2 at Ser-256 enhances its water permeability.

Body water homeostasis is essential for the survival of mammals and is regulated by the renal collecting duct. Key components in the regulation of collecting duct water permeability are the vasopressin receptor and the water channel aquaporin-2 (AQP2)[2] (1–6). Mutations in the vasopressin V_2 receptor and AQP2 cause congenital nephrogenic diabetes insipidus, a disease characterized by a massive loss of water through the kidney (7, 8). The binding of the antidiuretic hormone vasopressin to vasopressin V_2 receptors on renal principal cells stimulates cAMP synthesis via activation of adenylate cyclase. The subsequent activation of PKA leads to phosphorylation of AQP2 at Ser-256, and this phosphorylation event is required to increase the water permeability and water reabsorption of renal principal cells. It has been established that the phosphorylation of AQP2 induces its apical membrane insertion, rendering the cell water-permeable. We showed recently that AQP2 binds to a multiprotein "motor" complex and that phosphorylation-dependent reciprocal interaction with G-actin and tropomyosin 5b directs AQP2 to the apical membrane (9–13). However, whether this phosphorylation regulates the water permeability of individual AQP2 proteins still remains unclear.

Kuwahara *et al.* (14) showed that cAMP stimulation increased the water permeability of AQP2 expressed in *Xenopus* oocytes, although this stimulation did not increase the amount of AQP2 on the oocyte membrane. This finding suggests that cAMP-mediated phosphorylation of AQP2 increases the water permeability of individual AQP2 proteins. On the other hand, Lande *et al.* (15) purified endosomes derived from the apical membrane of rat inner medullary collecting duct cells that were highly enriched for AQP2 and showed that their water permeability was not changed by AQP2 phosphorylation. However, it was not excluded that other proteins contained in oocytes or endosomes prepared from inner medullary collecting duct cells may have affected these responses. For example, basal phosphorylation levels of AQP2 determined by endogenous kinase or phosphatase activities may affect the results in these experimental systems. To clarify whether the water permeability of AQP2 is regulated by its phosphorylation event alone, an experimental system that does not contain other regulatory proteins is required.

In this study, we performed large-scale expression of full-length recombinant human AQP2, purified it, reconstituted it into proteoliposomes, and examined the protein function. Here, we show the direct evidence that the water permeability of AQP2 is regulated by its phosphorylation at Ser-256 by PKA.

EXPERIMENTAL PROCEDURES

Expression and Purification of Recombinant AQP2—Human AQP2 cDNA was subcloned into pET32 (Novagen, Madison, WI) to generate His-tagged thioredoxin (Trx)-fused AQP2 (AQP2/Trx). AQP2 mutants were generated by PCR using a QuikChange II site-directed mutagenesis kit (Stratagene, La Jolla, CA) and the following sense primers: I, 5′-GTGCGACGGCGGCAGGCGGTGGAGCTGCACTCG-3′; II, 5′-GTGCGACGGCGGCAGGACGTGGAGCTGCACTCG-

* This work was supported in part by Grants-in-aid 17GS0312 and 21591053 from the Japan Society for the Promotion of Science.

[1] To whom correspondence should be addressed: Dept. of Nephrology, Tokyo Medical and Dental University, 1-5-45 Yushima, Bunkyo-ku, Tokyo 113-8519, Japan. Tel.: 81-3-5803-5214; Fax: 81-3-5803-5215; E-mail: ynodmed2@tmd.ac.jp.

[2] The abbreviations used are: AQP2, aquaporin-2; Trx, thioredoxin.

3′; III, 5′-TCGGTGGAGCTGCACGCGCCGCAGAGCCTG-CCA-3′; IV, 5′-TCGGTGGAGCTGCACGACCCGCAGAG-CCTGCCA-3′; V, 5′-CTGCACTCGCCGCAGGCGCTGCC-ACGGGGTACC-3′; VI, 5′-GCGGTGGAGCTGCACGCGC-CGCAGAGCCTGCCA-3′; VII, 5′-CTGCACGCGCCGCAG-GCGCTGCCACGGGGTACC-3′; and VIII, 5′-CTGCCACG-GGGTGCGAAGGCCTGAAAGCTT-3′. The S256A and S256D mutants were generated from WT-AQP2 using primers I and II, respectively. The S261A and S261D mutants were generated from WT-AQP2 using primers III and IV, respectively. The S256A/S261A/S264A mutant was generated using primer VII from S256A/S261A, which was generated from S256A using primer VI. The S256A/S261A/S264A/T269A mutant was generated from S256A/S261A/S264A using primer VIII. The S256A/S261A/T269A mutant was generated from S256A/S261A using primer VIII. The S256A/S264A/T269A mutant was generated using primer VIII from S256A/S264A, which was generated from S256A using primer V. The S261A/S264A/T269A mutant was generated using primer VIII from S261A/S264A, which was generated from S261A using primer VII.

WT-AQP2/Trx and Mutants were expressed in *Escherichia coli* BL21 (Novagen) by induction with 1 mM isopropyl-β-D-thiogalactopyranoside for 4 h at 30 °C. The bacterial pellets were incubated with lysozyme, sonicated, and centrifuged at 10,000 × *g*. For AQP2 purification, the pellets were suspended with 6 M urea in PBS and centrifuged. The supernatants were diluted to a concentration of 2 M urea and applied to a column of TALON resin (Clontech). The column was washed and eluted by buffer A (50 mM K-HEPES (pH 7.6), 100 mM KCl, and 10 mM $MgCl_2$) containing 2% octyl glucoside and 150 mM imidazole. AQP2 purification was confirmed by Coomassie Blue staining, silver staining, and immunoblotting using anti-AQP2 antibody, which was generated against a synthetic peptide corresponding to 15 C-terminal amino acid residues (positions 257–271) of AQP2 (12, 16). For PKA phosphorylation, AQP2 protein was added with 1 mM ATP and 200,000 units/ml cAMP-dependent PKA (New England Biolabs, Beverly, MA) and incubated at 30 °C for 1 h. The phosphorylation was confirmed by immunoblotting using antibodies for AQP2 phosphorylated at Ser-256 (12, 17). Antibodies for AQP2 phosphorylated at Ser-256 were generated against a synthetic peptide corresponding to amino acids 253–262 of human AQP2, with the addition of a cysteine residue at the C terminus and a glycine residue at the N terminus, which was phosphorylated at Ser-256, as described previously (18, 19).

Measurement of the Sites and Efficiency of Phosphorylation by PKA in Recombinant Human AQP2—The phosphorylation sites and efficiency were measured as described previously (20, 21) with the following modifications. A synthetic phosphopeptide corresponding to the C terminus of AQP2 (residues 231–271) that was phosphorylated at Ser-256 was used as a standard. As shown in Fig. 3*D*, WT-AQP2 and mutant proteins and the phosphopeptide standard were immunoblotted using antibodies for phosphoserine (Sigma) to examine their phosphorylation efficiencies. A dot blot was prepared by spotting 25 pmol (2 μl) of each AQP2 protein and the phosphopeptide standard onto a nitrocellulose membrane. The membrane was then processed as for Western blot analysis. Coomassie Blue staining was performed to confirm that the loaded molar amounts were equal among WT-AQP2 and mutant proteins.

Reconstitution of Recombinant AQP2 into Liposomes—Lipids (Sigma) were mixed in chloroform/methanol (2:1, v/v) to yield phosphatidylcholine (molar ratio of 1) and cholesterol (molar ratio of 1.6). After drying under N_2 gas, they were resuspended in buffer A containing 2% octyl glucoside to a total lipid concentration of 7.5 mM, mixed with an equal volume of recombinant AQP2 (0.7 mg/ml), and dialyzed against 50 mM Tris-HCl (pH 7.5) and 10 mM $MgCl_2$. The proteoliposomes were overlaid with step gradients of 30 and 40% OptiPrep (Axis-Shield, Oslo, Norway) and centrifuged using an SW41Ti rotor (Beckman Coulter, Fullerton, CA) at 39,000 rpm for 4 h. The proteoliposomes were collected at the 0–30% interface and extruded through polycarbonate filters with 50-nm pores using a LiposoFast extruder (Avestin, Ottawa, Canada) to obtain unilamellar vesicles (22).

Measurement of Osmotic Water Permeability—The stopped-flow experiments were performed on an Applied Photophysics SX18.MV stopped-flow apparatus. The proteoliposomes suspended in 50 mM Tris-HCl (pH 7.5) containing 1 mM DTT were abruptly mixed with 50 mM Tris-HCl (pH 7.5) containing 600 mM mannitol, and the liposomes were imposed with a 300 mM inwardly directed osmotic gradient. To inhibit the water transport of AQP2, AQP2-incorporated liposomes (AQP2-liposomes) were treated with 1 mM $HgCl_2$ for 15 min. A decrease in the liposome volume due to osmotic water efflux driven by the osmotic gradient was monitored as the time-dependent increase in 90° scattered light intensity monitored at 466 nm. The data were fitted to a double exponential function. The osmotic water permeability (P_f) was calculated from the initial rate of volume change by the relation $dV(t)/dt = P_f SAV \cdot V_W(Osm_{out} - Osm_{in})$, where $V(t)$ is liposome volume at time t, SAV is initial surface area to volume ratio (calculated from the liposome diameter examined by electron microscopy), V_W is the molar volume of water (18×10^{-3} liters/mol), and $Osm_{out} - Osm_{in}$ is the difference in external and internal osmolarity.

Statistical Analysis—All values are expressed as means ± S.E. Data were analyzed by one-way analysis of variance, followed by the Bonferroni test for multiple comparisons, and $p < 0.05$ was considered to be statistically significant. All statistical procedures were carried out using SPSS Version 11.5 (SPSS Inc., Chicago, IL).

RESULTS

Expression and Purification of Recombinant WT-AQP2 and Mutants—To examine the regulation of the water permeability of AQP2 by its phosphorylation without the effects of other regulatory proteins, we performed large-scale expression of full-length recombinant human AQP2 fused to Trx and purified it (Fig. 1*A*). A single band corresponding to the theoretical size of 49 kDa was recognized by both Coomassie Blue staining and immunoblotting using anti-AQP2 antibody, confirming that the purified recombinant protein preparation

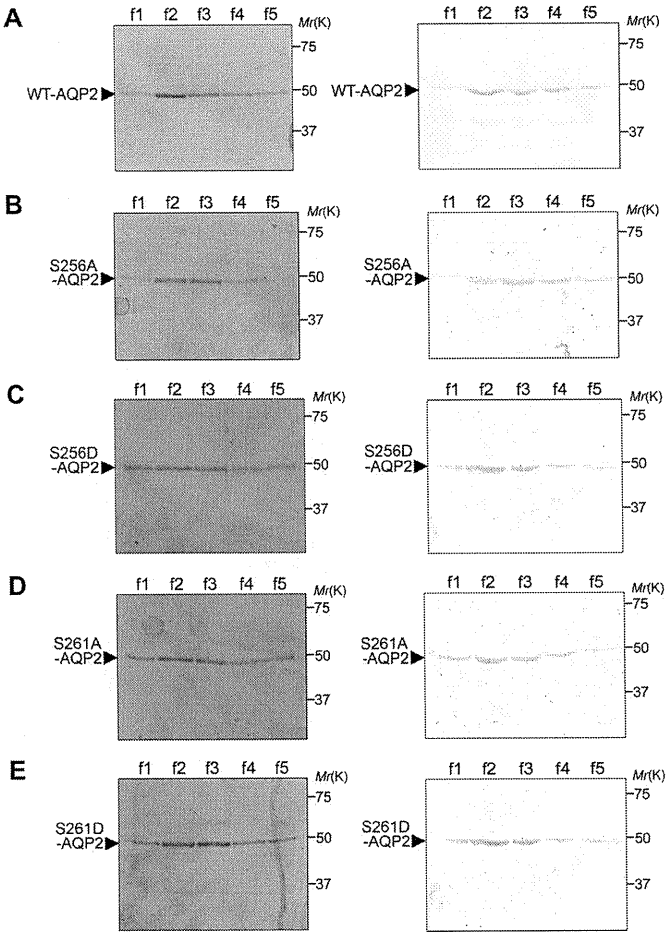

FIGURE 1. **Purification of recombinant WT-AQP2 and mutants.** Full-length human WT-AQP2 (*A*), S256A-AQP2 (*B*), S256D-AQP2 (*C*), S261A-AQP2 (*D*), and S261D-AQP2 (*E*) were fused to Trx; expressed in *E. coli* BL21; purified using a TALON metal affinity column; separated by SDS-PAGE; and subjected to Coomassie Blue staining (*left panels*) and immunoblotting using anti-AQP2 antibody (*right panels*). *Lanes f1–f5* indicate consecutive serial elution fractions (5 × 500 μl) of 1 ml of the TALON matrix column.

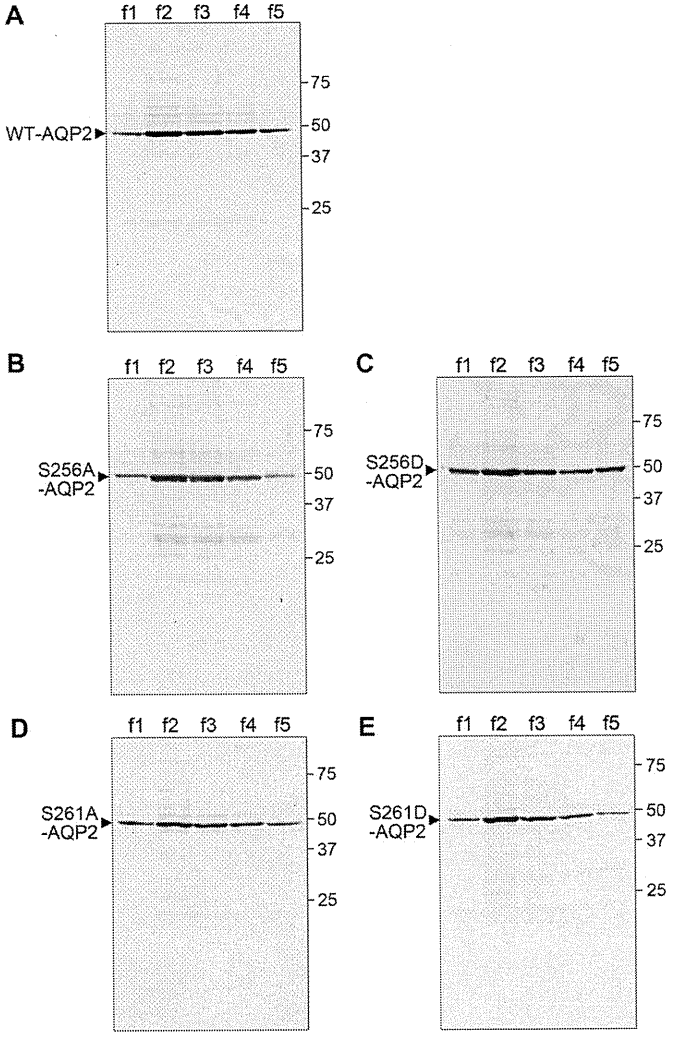

FIGURE 2. **Silver staining of recombinant WT-AQP2 and mutants.** Purified WT-AQP2 (*A*), S256A-AQP2 (*B*), S256D-AQP2 (*C*), S261A-AQP2 (*D*), and S261D-AQP2 (*E*) were separated by SDS-PAGE and subjected to silver staining. *Lanes f1–f5* indicate consecutive serial elution fractions (5 × 500 μl), and 35 μl from each fraction was loaded.

was indeed AQP2. To further confirm the purity of this protein, silver staining was performed (Fig. 2*A*). There were faint nonspecific protein bands. Densitometric analysis showed that the purity of AQP2 protein was >95%. To examine the roles of phosphorylation at Ser-256 and Ser-261, we also expressed and purified mutants mimicking the phosphorylated (S256D and S261D) and non-phosphorylated (S256A and S261A) states. In addition to Ser-256, phosphorylation at Ser-261 is also regulated by vasopressin, and its roles have been examined (17, 23–25). Coomassie Blue staining and immunoblotting using anti-AQP2 antibody showed the purification of these mutants (Fig. 1, *B–E*). Silver staining further confirmed that these mutant proteins were of high purity (Fig. 2, *B–E*).

Phosphorylation of AQP2 by PKA—WT-AQP2 was then subjected to *in vitro* PKA phosphorylation. Immunoblotting for total AQP2 and phosphorylated AQP2 confirmed AQP2 phosphorylation (Fig. 3, *A* and *B*).

We then examined the sites and efficiencies of phosphorylation of recombinant human AQP2 by PKA (Fig. 3, *C* and *D*). Recent phosphoproteome analyses have shown that three other sites are also phosphorylated in addition to Ser-256, although Ser-256 is phosphorylated predominantly in rat renal inner medullary collecting duct cells (20, 23). Ser-256 phosphorylation is most likely mediated by PKA (3, 26), whereas the kinases acting at the other sites have not been reported. To confirm the sites phosphorylated by PKA in recombinant human AQP2, we expressed and purified non-phosphorylation-mimicking mutants at plausible phosphorylation sites: Ser-256, Ser-261, Ser-264, and Thr-269. Coomassie Blue staining of 25 pmol each of WT-AQP2 and mutants, with or without phosphorylation by PKA, is shown in Fig. 3*C*. The band densities were equal, confirming that the loaded molar amounts were equal. In the immunoblot for phosphoserine, the signal of WT-AQP2 phosphorylated by PKA was similar to that of an equimolar amount of phosphopeptide, indicating that almost all WT-AQP2 was phosphorylated (Fig. 3*D*). Furthermore, the signal of the phosphorylated S261A/S264A/T269A-AQP2 mutant, in which Ser-256 was intact, was equal to those of phosphorylated WT-AQP2 and the phosphopeptide. On the other hand, positive

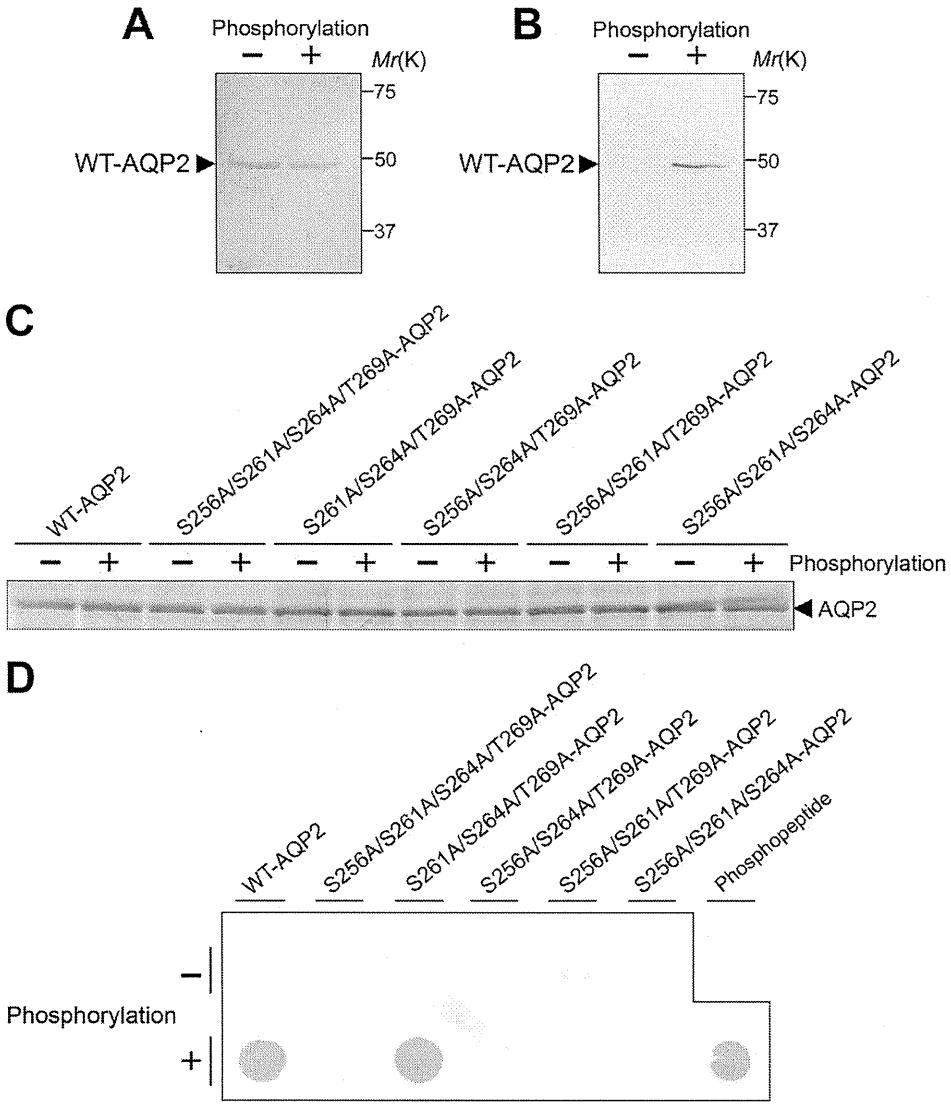

FIGURE 3. ***In vitro* phosphorylation of AQP2 by PKA.** *A* and *B*, WT-AQP2 with or without phosphorylation was immunoblotted using anti-AQP2 antibody (*A*) and anti-phosphorylated AQP2 antibody (*B*). Anti-AQP2 antibody was generated against a synthetic peptide corresponding to 15 C-terminal amino acid residues (positions 257–271) of AQP2. Anti-phosphorylated AQP2 antibody was generated against a synthetic peptide corresponding to amino acids 253–262 of AQP2 with phosphorylation at Ser-256. Details are provided under "Experimental Procedures." *C* and *D*, sites and efficiency of phosphorylation by PKA in AQP2. *C*, WT-AQP2 and mutant proteins (25 pmol each), with or without phosphorylation by PKA, were analyzed by SDS-PAGE and Coomassie Blue staining. *D*, WT-AQP2 and mutant proteins (25 pmol each), with or without phosphorylation by PKA, and the phosphopeptide standard were subjected to dot blot analysis using antibodies for phosphoserine.

signals were not detected for any mutants that included the S256A mutation. These findings indicate that only Ser-256 in recombinant AQP2 is phosphorylated by PKA.

Reconstitution of AQP2 into Liposomes—WT-AQP2 and mutants were reconstituted into proteoliposomes as described under "Experimental Procedures." Proteins that were not reconstituted into liposomes were removed by fractionating on OptiPrep step gradients (Fig. 4*A*). The proteoliposomes were extruded through polycarbonate filters to obtain unilamellar vesicles (22). The size of the proteoliposomes was examined by negative stain electron microscopy (Fig. 4*B*). The diameter was similar in different kinds of liposomes: liposomes without protein reconstitution, 185 ± 4 nm; Trx-liposomes, 193 ± 5 nm; non-phosphorylated WT-AQP2-liposomes, 200 ± 4 nm; phosphorylated WT-AQP2-liposomes, 199 ± 5 nm; S256A-AQP2-liposomes, 189 ± 4 nm; S256D-AQP2-liposomes, 190 ± 4 nm; S261A-AQP2-liposomes, 200 ± 4 nm; and S261D-AQP2-liposomes, 196 ± 6 nm.

PKA Phosphorylation of AQP2 Enhances Its Water Permeability—We then examined the P_f of WT-AQP2-liposomes, Trx-liposomes, and liposomes without protein reconstitution (Fig. 5). The P_f of non-phosphorylated WT-AQP2-liposomes was significantly greater than that of the control substances, which were Trx-liposomes and liposomes without protein incorporation. Treatment of WT-AQP2-liposomes with $HgCl_2$ significantly decreased their P_f to the control levels. This finding indicates that the increased P_f of AQP2-liposomes is mediated by the AQP2 function of water transport. PKA phosphorylation significantly increased the water permeability of WT-AQP2-liposomes. These findings indicate

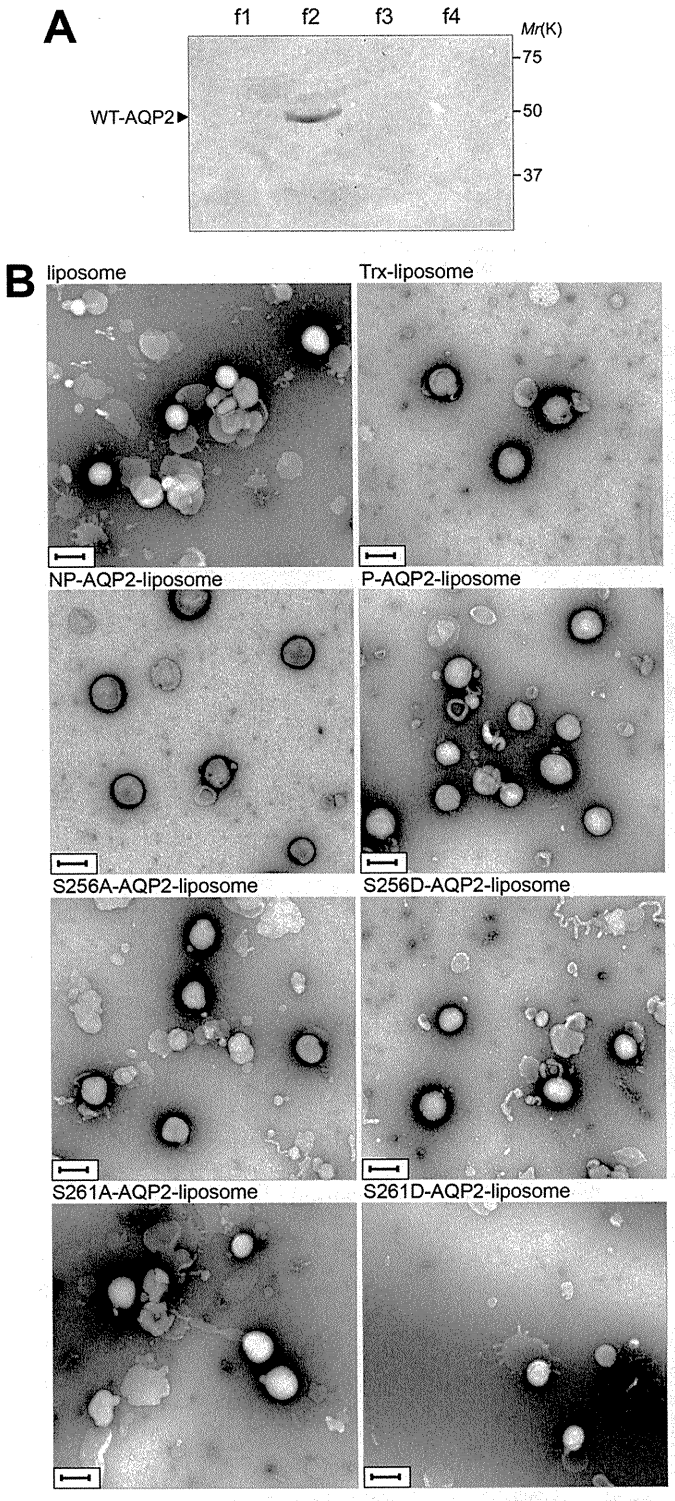

FIGURE 4. **Reconstitution of AQP2 into liposomes.** *A*, WT-AQP2 reconstituted in proteoliposomes was fractionated on OptiPrep step gradients, separated by SDS-PAGE, and immunoblotted using anti-AQP2 antibody. The OptiPrep concentrations in each fraction were 0% (*f1*), 0–30% interface (*f2*), 30% (*f3*), and 40% (*f4*). Proteoliposomes existed in the 0–30% OptiPrep interface. *B*, negative stain electron microscopy of liposome without protein incorporation, Trx-liposome, non-phosphorylated WT-AQP2-liposome (*NP-AQP2-liposome*), phosphorylated WT-AQP2-liposome (*P-AQP2-liposome*), S256A-AQP2-liposome, S256D-AQP2-liposome, S261A-AQP2-liposome, and S261D-AQP2-liposome, which were derived from the *f2* fraction. *Scale bars* = 200 nm.

that the water permeability of AQP2 is enhanced by its phosphorylation.

Phosphorylation of AQP2 at Ser-256 Is Essential for PKA Regulation of Its Water Permeability—We then examined the role of AQP2 phosphorylation in the regulation of P_f using phosphorylation mutants of AQP2 reconstituted into proteoliposomes (Fig. 6). The P_f of non-phosphorylation-mimicking mutant S256A-AQP2-liposomes was similar to that of non-phosphorylated WT-AQP2-liposomes. On the other hand, the P_f of phosphorylation-mimicking mutant S256D-AQP2-liposomes was significantly increased up to the levels of phosphorylated WT-AQP2-liposomes. PKA phosphorylation did not alter the P_f of either S256A-AQP2 or S256D-AQP2. These findings indicate that phosphorylation of AQP2 at Ser-256 is essential for PKA regulation of its water permeability and that phosphorylation at other sites in AQP2 is not involved in this regulation. Furthermore, the P_f values of both S261A and S261D mutants were similar to those of non-phosphorylated WT-AQP2, indicating that phosphorylation at Ser-261 has no effect on P_f.

DISCUSSION

This study provides direct evidence for the regulation of the water transport activity of AQP2 by phosphorylation. AQP2-regulated water reabsorption in kidney collecting ducts is a key event for the maintenance of body water balance. In addition to the intracellular translocation of AQP2 to the luminal membrane, our findings indicate that the water transport activity of individual AQP2 proteins is important for the regulation of water reabsorption in kidney collecting ducts.

To date, several groups have examined the role of phosphorylation in P_f. Kuwahara *et al.* (14) examined the phosphorylation and P_f of AQP2 expressed in *Xenopus* oocytes. They showed that PKA phosphorylated AQP2 at Ser-256. cAMP stimulation increased the P_f of oocytes expressing AQP2, although this stimulation did not increase the amount of AQP2 on the oocyte surface, which was examined by immunoblotting of AQP2 using oocyte membranes. This finding suggested that the P_f of individual AQP2 proteins was increased by cAMP-mediated phosphorylation of AQP2. However, the possibility of phosphorylation-induced translocation of AQP2 could not be excluded in this experimental system. Recently, Moeller *et al.* (27) also examined the role of phosphorylation using AQP2 expressed in *Xenopus* oocytes. To evaluate the P_f of a single channel, P_f relative to the plasma membrane abundance was compared among WT-AQP2 and mutants. Both the P_f and plasma membrane abundance of the non-phosphorylation-mimicking mutant S256A-AQP2 were decreased compared with those of WT-AQP2, resulting in the P_f relative to the plasma membrane abundance being similar. This finding suggested that a lack of phosphorylation at this site had no effect on individual AQP2 proteins. However, the methods determining the plasma membrane abundance were semi-quantitative, and this study could not exclude the possibility that the P_f of individual AQP2 proteins was altered by this mutation. On the other hand, Lande *et al.* (15) purified endosomes derived from the apical membrane of rat inner medul-

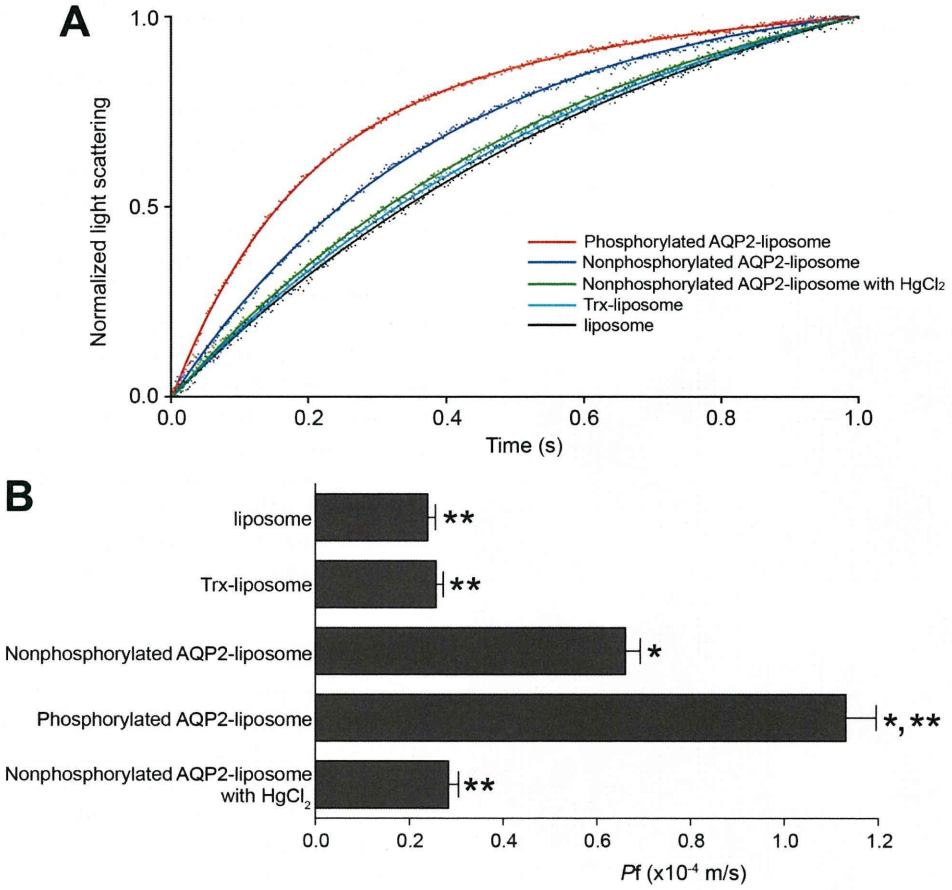

FIGURE 5. **PKA phosphorylation of AQP2 enhances its water permeability.** *A*, stopped-flow analysis. Proteoliposomes or liposomes without protein incorporation were abruptly imposed to an inwardly directed osmotic gradient, and the vesicle shrinkage was monitored by measuring the increase in scattered light. The *dots* are measured values, and the *solid lines* are their fitted curves. *Red*, phosphorylated WT-AQP2-liposome; *dark blue*, non-phosphorylated WT-AQP2-liposome; *green*, non-phosphorylated WT-AQP2-liposome treated with $HgCl_2$; *light blue*, Trx-liposome; *black*, liposome without protein incorporation. *B*, summary of osmotic water permeability (P_f). Data represent means ± S.E. from 15–20 independent experiments. *, $p < 0.001$ *versus* Trx-liposome; **, $p < 0.001$ *versus* non-phosphorylated AQP2-liposome.

lary collecting duct cells that were highly enriched for AQP2. These endosomes contained endogenous PKA and phosphatase activities that could phosphorylate and dephosphorylate AQP2. Therefore, these authors prepared two kinds of samples to detect the effect of phosphorylation on P_f. For phosphorylated AQP2, AQP2-endosomes were incubated with exogenous PKA catalytic subunit and ATP to maximize the phosphorylation levels. For non-phosphorylated AQP2, the above phosphorylated sample was then incubated with exogenous alkaline phosphatase, which was shown to remove 95% of the phosphate from AQP2. There was no significant difference in P_f between these two samples, suggesting that the P_f of AQP2 is not changed by its phosphorylation. However, the phosphorylation levels of AQP2-endosomes incubated with exogenous PKA and ATP progressively decreased over 20 min, which might have been caused by endogenous phosphatase activities. It is possible that the differences in P_f may have been underestimated due to the existence of endogenous PKA, phosphatase, and other regulatory proteins in AQP2-endosomes. Our experimental system using recombinant AQP2 reconstituted into liposomes did not contain any other proteins, and thus, the potential effects of other regulatory proteins were excluded. This provides direct evidence that phosphorylation of AQP2 regulates its water permeability.

In this study, it is possible that not all AQP2 proteins were reconstituted in liposomes with the proper orientation and topology, which may have caused underestimation of their water transport activity. However, significant water transport via AQP2 was observed, demonstrating functional reconstitution into liposomes, as shown in Fig. 5. Moreover, the effects of PKA phosphorylation and mutations of AQP2 on P_f were clearly observed (Figs. 5 and 6).

There is increasing evidence that aquaporins are gated (28). The spinach aquaporin SoPIP2;1 is gated by phosphorylation at Ser-115 and Ser-274 (29). Structural studies using electron diffraction (30) and x-ray crystallography (31) proposed the molecular mechanism of this gating. In the closed conformation, loop D caps the pore of this channel from the cytoplasm, preventing the water passage. In the open conformation, loop D is displaced, thereby unblocking the cytoplasmic entrance of the water pore. Molecular dynamic simulations indicate that Ser-115 phosphorylation triggers this movement of loop D (31). Furthermore, x-ray structural analysis of phosphorylation mutants suggests that phosphorylation at Ser-188 may also produce an open channel, which was supported by an

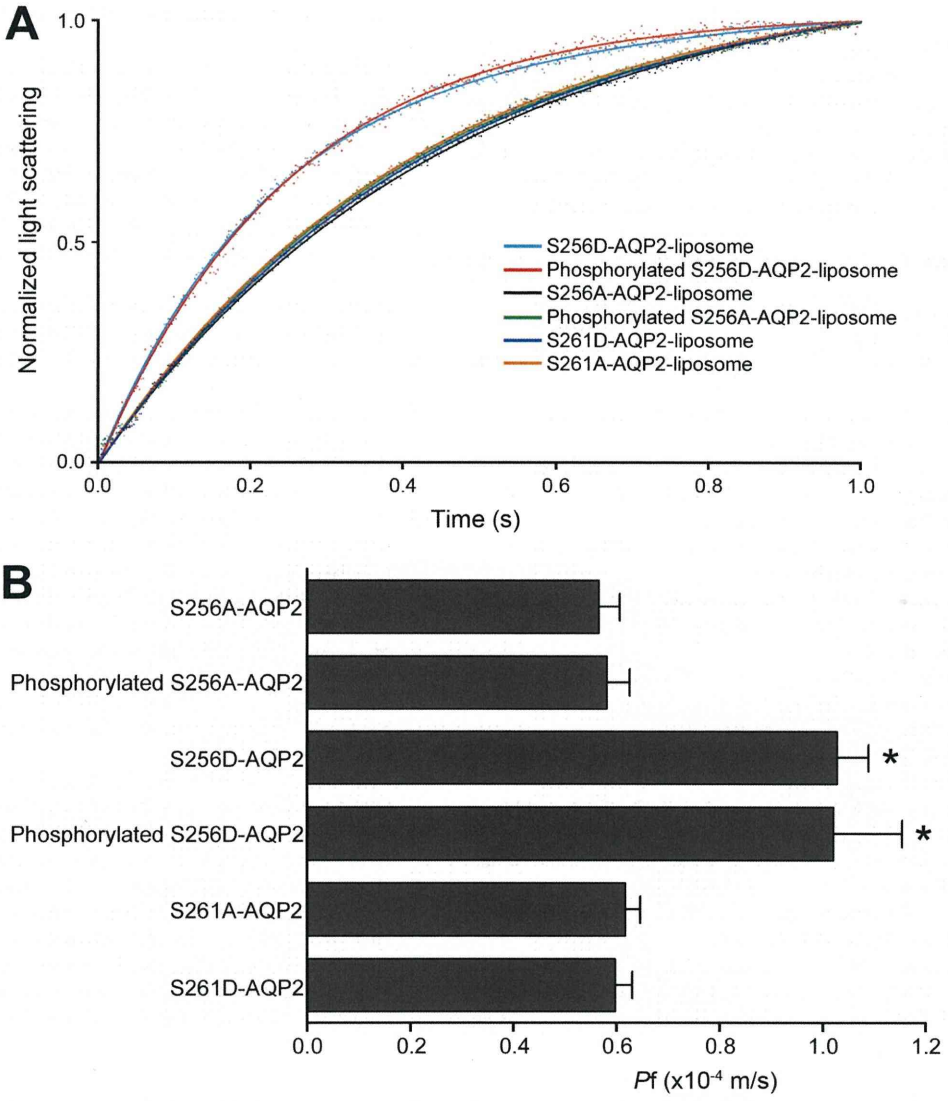

FIGURE 6. **Phosphorylation of AQP2 at Ser-256 is essential for PKA regulation of its water permeability.** *A*, stopped-flow analysis of phosphorylation mutants of AQP2 reconstituted into liposomes. *Light blue*, S256D-AQP2-liposome; *red*, PKA-phosphorylated S256D-AQP2-liposome; *black*, S256A-AQP2-liposome; *green*, PKA-phosphorylated S256A-AQP2-liposome; *dark blue*, S261D-AQP2-liposome; *orange*, S261A-AQP2-liposome. *B*, summary of P_f. Data represent means ± S.E. from 15–25 independent experiments. *, $p < 0.001$ *versus* S256A-AQP2-liposome.

increased water transport activity of this mutant and also molecular dynamics simulations (32). These simulations have revealed interactions between phosphorylated Ser-188 and Lys-270 of the C terminus that lead to a conformational change in loop D and channel opening. This finding also indicates an important role for the C terminus of aquaporin in the gating mechanism.

AQP4 is the predominant water channel in the mammalian brain, and its water permeability is also regulated by its phosphorylation. The water permeability of AQP4 is decreased by its phosphorylation at Ser-180 by protein kinase C (33) and is enhanced by phosphorylation at Ser-111 by protein kinase G (34). Electron crystallography of double-layered, two-dimensional crystals suggests a mechanism that phosphorylated Ser-180 may bind to the C-terminal domain, which blocks the cytoplasmic entrance of this water channel (35).

The yeast aquaporin Aqy1 has also been shown to be a gated channel by x-ray structural analysis at 1.15 Å (36). The extended N terminus caps the water channel entrance. Furthermore, molecular dynamics simulations and functional studies have suggested that its water transport activity is regulated by mechanosensitivity and Ser-107 phosphorylation (36).

We have shown here that the water transport activity of AQP2 is regulated by phosphorylation at Ser-256, which is located in the cytoplasmic C-terminal domain. Although a crystal structure of AQP2 has not been reported to date, we speculate that this phosphorylation induces conformational changes in the C terminus that are important for channel gating. Structural analysis is required to further characterize the molecular details of AQP2 gating.

Acknowledgments—We thank Prof. Kaoru Mitsuoka and Drs. Nobuhiko Gyobu and Daisuke Kasuya (National Institute of Advanced Industrial Science and Technology) for teaching us the electron microscopic technique and observation.

REFERENCES

1. Fushimi, K., Uchida, S., Hara, Y., Hirata, Y., Marumo, F., and Sasaki, S. (1993) *Nature* **361,** 549–552
2. Nielsen, S., Frøkiaer, J., Marples, D., Kwon, T. H., Agre, P., and Knepper, M. A. (2002) *Physiol. Rev.* **82,** 205–244
3. Noda, Y., and Sasaki, S. (2006) *Biochim. Biophys. Acta* **1758,** 1117–1125
4. Boone, M., and Deen, P. M. (2008) *Pflugers Arch.* **456,** 1005–1024
5. Brown, D., Breton, S., Ausiello, D. A., and Marshansky, V. (2009) *Traffic* **10,** 275–284
6. Hoffert, J. D., Chou, C. L., and Knepper, M. A. (2009) *J. Biol. Chem.* **284,** 14683–14687
7. Loonen, A. J., Knoers, N. V., van Os, C. H., and Deen, P. M. (2008) *Semin. Nephrol.* **28,** 252–265
8. Noda, Y., Sohara, E., Ohta, E., and Sasaki, S. (2010) *Nat. Rev. Nephrol.* **6,** 168–178
9. Noda, Y., Horikawa, S., Katayama, Y., and Sasaki, S. (2004) *Biochem. Biophys. Res. Commun.* **322,** 740–745
10. Noda, Y., Horikawa, S., Furukawa, T., Hirai, K., Katayama, Y., Asai, T., Kuwahara, M., Katagiri, K., Kinashi, T., Hattori, M., Minato, N., and Sasaki, S. (2004) *FEBS Lett.* **568,** 139–145
11. Noda, Y., Horikawa, S., Katayama, Y., and Sasaki, S. (2005) *Biochem. Biophys. Res. Commun.* **330,** 1041–1047
12. Noda, Y., Horikawa, S., Kanda, E., Yamashita, M., Meng, H., Eto, K., Li, Y., Kuwahara, M., Hirai, K., Pack, C., Kinjo, M., Okabe, S., and Sasaki, S. (2008) *J. Cell Biol.* **182,** 587–601
13. Noda, Y., and Sasaki, S. (2008) *Pflugers Arch.* **456,** 737–745
14. Kuwahara, M., Fushimi, K., Terada, Y., Bai, L., Marumo, F., and Sasaki, S. (1995) *J. Biol. Chem.* **270,** 10384–10387
15. Lande, M. B., Jo, I., Zeidel, M. L., Somers, M., and Harris, H. W., Jr. (1996) *J. Biol. Chem.* **271,** 5552–5557
16. Yamashita, Y., Hirai, K., Katayama, Y., Fushimi, K., Sasaki, S., and Marumo, F. (2000) *Am. J. Physiol. Renal Physiol.* **278,** F395–F405
17. Li, Y. H., Eto, K., Horikawa, S., Uchida, S., Sasaki, S., Li, X. J., and Noda, Y. (2009) *Int. J. Biochem. Cell Biol.* **41,** 2466–2476
18. Christensen, B. M., Zelenina, M., Aperia, A., and Nielsen, S. (2000) *Am. J. Physiol. Renal Physiol.* **278,** F29–F42
19. Nishimoto, G., Zelenina, M., Li, D., Yasui, M., Aperia, A., Nielsen, S., and Nairn, A. C. (1999) *Am. J. Physiol. Renal Physiol.* **276,** F254–F259
20. Xie, L., Hoffert, J. D., Chou, C. L., Yu, M. J., Pisitkun, T., Knepper, M. A., and Fenton, R. A. (2010) *Am. J. Physiol. Renal Physiol.* **298,** F1018–F1023
21. Higashimoto, Y., Saito, S., Tong, X. H., Hong, A., Sakaguchi, K., Appella, E., and Anderson, C. W. (2000) *J. Biol. Chem.* **275,** 23199–23203
22. MacDonald, R. C., MacDonald, R. I., Menco, B. P., Takeshita, K., Subbarao, N. K., and Hu, L. R. (1991) *Biochim. Biophys. Acta* **1061,** 297–303
23. Hoffert, J. D., Pisitkun, T., Wang, G., Shen, R. F., and Knepper, M. A. (2006) *Proc. Natl. Acad. Sci. U.S.A.* **103,** 7159–7164
24. Hoffert, J. D., Nielsen, J., Yu, M. J., Pisitkun, T., Schleicher, S. M., Nielsen, S., and Knepper, M. A. (2007) *Am. J. Physiol. Renal Physiol.* **292,** F691–F700
25. Lu, H. J., Matsuzaki, T., Bouley, R., Hasler, U., Qin, Q. H., and Brown, D. (2008) *Am. J. Physiol. Renal Physiol.* **295,** F290–F294
26. Fushimi, K., Sasaki, S., and Marumo, F. (1997) *J. Biol. Chem.* **272,** 14800–14804
27. Moeller, H. B., MacAulay, N., Knepper, M. A., and Fenton, R. A. (2009) *Am. J. Physiol. Renal Physiol.* **296,** F649–F657
28. Hedfalk, K., Törnroth-Horsefield, S., Nyblom, M., Johanson, U., Kjellbom, P., and Neutze, R. (2006) *Curr. Opin. Struct. Biol.* **16,** 447–456
29. Johansson, I., Karlsson, M., Shukla, V. K., Chrispeels, M. J., Larsson, C., and Kjellbom, P. (1998) *Plant Cell* **10,** 451–459
30. Kukulski, W., Schenk, A. D., Johanson, U., Braun, T., de Groot, B. L., Fotiadis, D., Kjellbom, P., and Engel, A. (2005) *J. Mol. Biol.* **350,** 611–616
31. Törnroth-Horsefield, S., Wang, Y., Hedfalk, K., Johanson, U., Karlsson, M., Tajkhorshid, E., Neutze, R., and Kjellbom, P. (2006) *Nature* **439,** 688–694
32. Nyblom, M., Frick, A., Wang, Y., Ekvall, M., Hallgren, K., Hedfalk, K., Neutze, R., Tajkhorshid, E., and Törnroth-Horsefield, S. (2009) *J. Mol. Biol.* **387,** 653–668
33. Zelenina, M., Zelenin, S., Bondar, A. A., Brismar, H., and Aperia, A. (2002) *Am. J. Physiol. Renal Physiol.* **283,** F309–F318
34. Gunnarson, E., Zelenina, M., Axehult, G., Song, Y., Bondar, A., Krieger, P., Brismar, H., Zelenin, S., and Aperia, A. (2008) *Glia* **56,** 587–596
35. Hiroaki, Y., Tani, K., Kamegawa, A., Gyobu, N., Nishikawa, K., Suzuki, H., Walz, T., Sasaki, S., Mitsuoka, K., Kimura, K., Mizoguchi, A., and Fujiyoshi, Y. (2006) *J. Mol. Biol.* **355,** 628–639
36. Fischer, G., Kosinska-Eriksson, U., Aponte-Santamaría, C., Palmgren, M., Geijer, C., Hedfalk, K., Hohmann, S., de Groot, B. L., Neutze, R., and Lindkvist-Petersson, K. (2009) *PLoS Biol.* **7,** e1000130

References

1. Quirce S. Eosinophilic bronchitis in the workplace. *Curr Opin Allergy Clin Immunol* 2004;**4**:87–91.
2. Barranco P, Fernández-Nieto M, del Pozo V, Sastre B, Larco JI, Quirce S. Nonasthmatic eosinophilic bronchitis in a baker caused by fungal alpha-amylase and wheat flour. *J Investig Allergol Clin Immunol* 2008;**18**:494–495.
3. Moscato G, Vandenplas O, Gerth Van Wijk R, Malo JL, Quirce S, Walusiak J et al. EAACI Task Force on Occupational Rhinitis. Occupational rhinitis. *Allergy* 2008;**63**:969–980.
4. Tarlo SM, Balmes J, Balkissoon R, Beach J, Beckett W, Bernstein D et al. Diagnosis and management of work-related asthma: American College Of Chest Physicians Consensus Statement. *Chest* 2008;**134**: 1S–41S.
5. Pignatti P, Pala G, Pisati M, Perfetti L, Banchieri G, Moscato G. Nasal blown secretion evaluation in specific occupational nasal challenges. *Int Arch Occup Environ Health* 2009 [Epub ahead of print] DOI:10.1007/s00420-009-0459-9.
6. Sturm GJ, Kranzelbinder B, Sturm EM, Heinemann A, Groselj-Strele A, Aberer W. The basophil activation test in the diagnosis of allergy: technical issues and critical factors. *Allergy* 2009;**64**:1319–1326.

Effects of nonsedative antihistamines on productivity of patients with pruritic skin diseases

H. Murota,* S. Kitaba, M. Tani, M. Wataya-Kaneda, I. Katayama

Keywords: antihistamine; itch; quality of life; skin diseases; WPAI-AS.

The symptoms associated with allergic diseases are recognized to exert a negative social and economic impact on patients as a result of impairments in work productivity (1, 2). Similar negative effects are experienced by patients with skin diseases such as chronic idiopathic urticaria, psoriasis, and chronic hand dermatitis (3–5). However, the consequences of pruritic skin diseases on productivity at work, in the classroom, and in daily activities are not fully understood. We assessed the impact of pruritic skin disease (e.g., dermatitis/eczema, urticaria, atopic dermatitis (AD), pruritus cutaneous) – as well as the effect of antihistamine therapy – on work, classroom, and daily productivity. In addition, we evaluated the effects of antihistamines on the intensity of itch and patient's quality of life (QOL).

Impaired work productivity in patients with pruritic skin diseases is improved significantly by nonsedative antihistamines.

The study design was approved by the Institutional Review Board, and patients with pruritic skin diseases (n = 206; male : female = 93 : 113; mean age ± SD: 52 ± 20 years) gave informed consent to participate in this study. Participants received no medical attention during the week before study initiation. The selection of therapy for each patient – i.e., oral antihistamines versus external medicine (e.g., steroid ointments, tacrolimus ointments, and certain moisturizers) – was left to the physician's discretion (open-label trial). The antihistamines fexofenadine (n = 72) and loratadine (n = 2), for which the package insert contained no cautionary statement regarding sedative actions, were categorized as 'nonsedative'. All other antihistamines were classified as 'sedative'. The effects of pruritic skin diseases on QOL were measured using the Skindex-16 instrument, and the magnitude of the itch sensation was assessed using a visual analog scale (VAS) (0–100). Work, classroom, and daily productivity were assessed by means of the Work Productivity-Activity Impairment-Allergy Specific (WPAI-AS) instrument (6). These instruments were self-administered by patients before (baseline) and 1 month after treatment initiation.

Based on the average baseline WPAI-AS scores for different diseases,

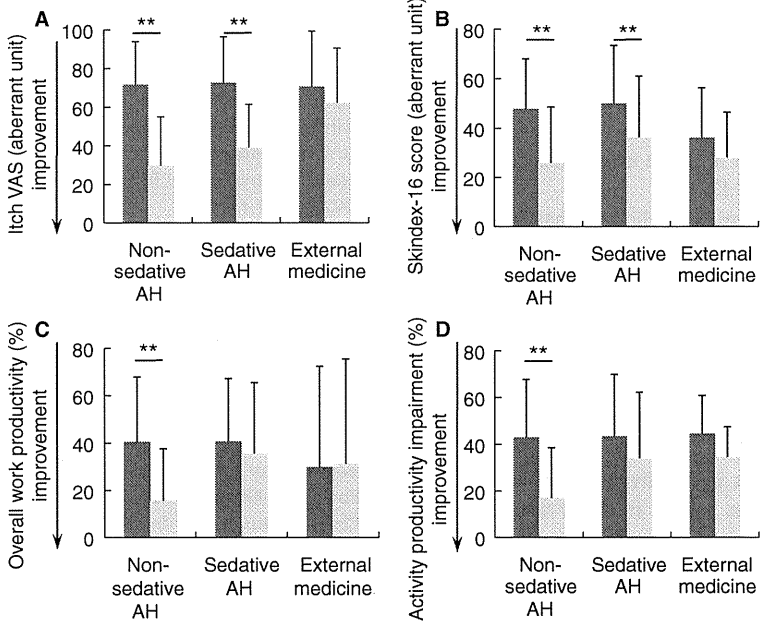

Figure 1 The impact of antihistamines on (A) itch visual analog scale, (B) skindex-16 score, (C) overall work productivity impairment, and (D) daily activity productivity impairment. The data for baseline (dark gray bars) and post-treatment assessment (light gray bars) are shown as mean ± SD. **Statistically significant improvement compared to baseline assessment (P < 0.001, one-sample t-test). AH, antihistamines.

pruritic skin diseases produced impairments in overall productivity in the workplace, classroom, and daily life activity of 39.3 ± 26.5%, 45.0 ± 28.9%, and 42.3 ± 25.1%, respectively. No significant differences between disease groups were identified at baseline. Patients in this study were treated for 1 month with oral antihistamines, with the exception of 11 patients who received only with topical medications. Nonsedative antihistamines were given to 74 patients, and the remaining 121 patients were treated with sedative antihistamines. The effects of these treatments on the intensity of itch, the Skindex-16 QOL score, overall work productivity, and daily activity productivity are shown in Fig. 1. As expected, itch intensity was reduced significantly by antihistamine therapy, while external medicines were ineffective (Fig. 1A). The effects of nonsedative and sedative antihistamines on itch intensity were similar (Fig. 1A). The effects of all treatments on the Skindex-16 QOL measure were similar to those for the itch VAS, with significant improvement from all antihistamines, but not for topical medications (Fig. 1B). As anticipated, impairments in overall work productivity and daily activity productivity were reduced significantly by nonsedative antihistamines, whereas sedative antihistamines failed to improve either measure (Fig. 1C,D).

Our results indicated that pruritic skin diseases negatively impact WPAI-AS scores at baseline. Sedative antihistamines fail to reduce work productivity impairment, despite decreasing itch VAS and Skindex-16 measures. Thus, clinicians should be aware of the potential to overestimate the benefits of sedative antihistamines on work productivity if they rely solely on patient intensity of itch and QOL values. In conclusion, this report highlights benefits in patient productivity as a new goal in the treatment of pruritic skin diseases and provides a rationale for shifting the choice of treatment to nonsedative antihistamines.

We thank Dr. Noriko Umegaki, Dr. Hiroaki Azukizawa, Dr. Atsushi Tanemura, Dr. Mika Terao, and Dr. Yorihisa Kotobuki for contributions to the data presented.

The authors have no conflict of interest.

*Department of Dermatology
Course of Integrated Medicine
Graduate School of Medicine
Osaka University
2-2 Yamadaoka, Suita
Osaka 5650871
Japan
Tel.: +81 66879 3031
Fax: +81 66879 3039
E-mail: h-murota@derma.med.osaka-u.ac.jp

Accepted for publication 7 October 2009
Allergy 2010: 65:929–930

DOI: 10.1111/j.1398-9995.2009.02262.x

References

1. Lamb CE, Ratner PH, Johnson CE, Ambegaonkar AJ, Joshi AV, Day D et al. Economic impact of workplace productivity losses due to allergic rhinitis compared with select medical conditions in the United States from an employer perspective. *Curr Med Res Opin* 2006;**22**: 1203–1210.
2. Okubo K, Gotoh M, Shimada K, Ritsu M, Okuda M, Crawford B. Fexofenadine improves the quality of life and work productivity in Japanese patients with seasonal allergic rhinitis during the peak cedar pollinosis season. *Int Arch Allergy Immunol* 2005;**136**:148–154.
3. Thompson AK, Finn AF, Schoenwetter WF. Effect of 60 mg twice-daily fexofenadine HCl on quality of life, work and classroom productivity, and regular activity in patients with chronic idiopathic urticaria. *J Am Acad Dermatol* 2000;**43**(1 Pt 1):24–30.
4. Pearce DJ, Singh S, Balkrishnan R, Kulkarni A, Fleischer AB, Feldman SR. The negative impact of psoriasis on the workplace. *J Dermatolog Treat* 2006;**17**:24–28.
5. Fowler JF, Ghosh A, Sung J, Emani S, Chang J, Den E et al. Impact of chronic hand dermatitis on quality of life, work productivity, activity impairment, and medical costs. *J Am Acad Dermatol* 2006;**54**:448–457.
6. Reilly MC, Tanner A, Meltzer EO. Work, classroom and activity impairment instruments: validation studies in allergic rhinitis. *Clin Drug Investig* 1996;**11**:278–288.

Maize: a new occupational allergen in the pharmaceutical industry

C.-M. Maniu, U. Faupel, G. Siebenhaar, N. Hunzelmann*

Keywords: excipient; maize; maize starch; occupational allergy.

Maize is part of contemporary nutrition and can be found in breakfast cereal, snacks, pastries, tortilla chips, polenta and many other foods. Moreover, maize flour and starch are often added to processed food, and starch is a widespread excipient of tablets. Allergic reactions to maize have previously been reported in southern Europe and Mexico where maize is commonly ingested. The major food allergen of maize, Zea m 14 is a heat-resistant lipid transfer protein and has a molecular weight of 9 kDa (1). Three other potential allergens have been detected: a 16-kDa α-amylase trypsin inhibitor, a thioredoxin named Zea m 25 (2) and a not yet characterized 50-kDa protein that belongs to the so-called reduced soluble protein fraction of the corn endosperm (3).

Maize starch should be considered as a potential occupational allergen in tablet manufacturing.

A 19-year-old girl, apprentice of a pharmaceutical company, noticed an erythematous itching rash on both hands and the face associated with dyspnea everyday 2 hours after starting work in tablet manufacturing. She was not known for any kind of seasonal or perennial allergic rhinoconjunctivitis, food or drug allergy, or atopic dermatitis.

Her company produces tablets of acetylsalicylic acid (ASA), nifedipin, acarbose, ciprofloxacin and moxifloxacin. Main excipients of these tablets are